

THE UNIVERSITY OF MICHIGAN  
INDUSTRY PROGRAM OF THE COLLEGE OF ENGINEERING

INITIAL CALIBRATION OF THE FORD NUCLEAR REACTOR

J. L. Shapiro  
W. F. Wegst  
A. H. Emmons  
H. J. Gomberg

June, 1958

IP-298



## TABLE OF CONTENTS

	<u>Page</u>
Summary of Important Results.....	1
Introduction.....	5
Lattice Configuration.....	6
Flux and Power Measurements.....	9
Rod Calibration.....	29
Temperature Coefficient.....	39
Reactivity Effects.....	45
Void Coefficient of Reactivity.....	47
Radiation Survey.....	53
Power Check at 100 kw.....	55
Temperatures at 100 kw.....	58
Conclusion.....	59
References.....	61
Appendix A - Other Critical Configurations.....	63
Appendix B - Flux and Power Data.....	65
Appendix C - Sample Power Calculation.....	77
Appendix D - Calculation of Void Ratio.....	81



## SUMMARY OF IMPORTANT RESULTS

### Critical Mass

The critical mass of the configuration shown in Figure 1 is 2497 gms. This aggregate is probably within 30 gms. of the minimum possible critical mass using the present safety and control rod pattern.

### Power Distribution

At low power (0.58 watts) the ratio of peak to average power is 1.6. The maximum power per gram of  $U^{235}$  is located at the middle of control element A and is 0.36 milliwatts/gm.

### Rod Calibration

The following are the rod worths for the configuration in Figure 1:

Control Rod:	0.29 percent	$\Delta k/k$
Safety A:	3.53 percent	$\Delta k/k$
Safety B:	3.77 percent	$\Delta k/k$
Safety C:	1.94 percent	$\Delta k/k$

### Temperature Coefficient

The temperature coefficient (Figure 10) is not constant.

Representative values are:

- $-4.3 \times 10^{-5}$  ( $\Delta k/k$ ) / $^{\circ}$ F at 70 $^{\circ}$ F
- $-5.5 \times 10^{-5}$  ( $\Delta k/k$ ) / $^{\circ}$ F at 90 $^{\circ}$ F
- $-7.0 \times 10^{-5}$  ( $\Delta k/k$ ) / $^{\circ}$ F at 110 $^{\circ}$ F

### Void Coefficient

The void coefficient of reactivity is a function of position and amount of void introduced, as illustrated in the table which follows. The maximum value is found at lattice position 35; the minimum, at lattice position 48. The average was calculated by weighting the coefficient for each lattice position by its power output.

Void Coefficient: $\Delta k/k$ per cc of void		
	1 percent void	6 percent void
Maximum	$-8.56 \times 10^{-6}$	$-5.50 \times 10^{-6}$
Minimum	$-4.55 \times 10^{-6}$	$-2.46 \times 10^{-6}$
Average	$-6.41 \times 10^{-6}$	$-4.05 \times 10^{-6}$

### Beam Port Reactivity Worth

For the configuration in Figure 1, the total effect of flooding all of the beam ports is the addition of 0.031 percent  $\Delta k/k$ .

### Radiation Survey

Radiation levels were measured in the building with the reactor operating at 100 kw. Significant values are tabulated below:

<u>General Location</u>	<u>mr/hr</u>	<u>Specific Location</u>
Third Floor	1.6	Water surface above reactor core
Second Floor	0	No detectable readings above background
First Floor	0.02	All port faces
Basement	0 5000	Entrance Door Pneumatic tube bundle entrance to pool (This was the highest value detected).

### Temperature at 100 kw

Water temperatures in the core with convection cooling at 100 kw were fairly uniform for all lattice positions. The low was 73°F at the bottom and the high, 102°F at the top.

### Conclusions

Measurements of the basic characteristics of the reactor show no indications of dangerous levels of temperature or radiation nor is there any indication of lack of stability. On the contrary, both the temperature and void coefficient measurements imply a substantial margin of inherent safety.

Although much future work will be done at power levels lower than 100 kw, the reactor staff recommends that the operating limit be raised to 1 Mw to increase the research capacity of the FNR.





## Introduction

The Ford Nuclear Reactor is located on the North Campus of the University of Michigan. This pool-type reactor, designed for operation at power levels of one megawatt, is being utilized for research and education. Descriptions of the reactor, and associated facilities, have been given in various publications. (12 - 16)

Initial criticality was attained September 18, 1957. Immediately following attainment of criticality, a program of calibration experiments at low power (0 - 10 watts) was initiated. These calibration experiments included measurements of flux distribution, rod worths, reactivity coefficients associated with temperature change, void formation, and flooding of beam ports. After completion of these low power experiments, the reactor power was raised to 100 kilowatts. Measurements of radiation levels inside the tank and outside the shield and also measurements of core temperatures were then made.

This program was instituted to procure the information necessary to calibrate the reactor instrumentation and to evaluate the operational and safety characteristics of the reactor. The report which follows provides details regarding the techniques and results of these calibrations.

## I. Lattice Configuration

During all of the low power calibration experiments only one configuration was used. Figure 1 shows this configuration. The numbers in the squares are the grid positions which are referred to throughout this report.

All the fuel elements are 18 plate (140 gm of  $U^{235}$ ) standard MTR elements, except for the four control elements which have 5 plates each (39 gms. of  $U^{235}$ ).

Besides the fission chamber, which is located in lattice position 31, there are four ion chambers (2 PCP, 2 CIC) located directly above lattice positions 23, 33, 43, and 53. These chambers were inserted to their lowest positions for the experiments. The amplification of the Log N amplifier, as well as that of the two level-safety amplifiers, was increased by a factor of 10 to provide better control and safety at low power.

Some other configurations, for which the critical mass has been evaluated, are shown in Appendix A.

A gross value for the critical mass, determined from the inverse multiplication plot, was found to be between 2400 grams and 2539 grams. A more precise value for the critical mass was subsequently calculated from the excess reactivity in the core. The excess reactivity was determined from the positions of the control and safety rods at criticality. These rod calibrations are described in Section III of this report.

Method: The excess reactivity in the core with all rods withdrawn is 0.406 percent.

Using the equation: (1)

$$\frac{\delta k_{\text{eff}}}{k_{\text{eff}}} = \left[ 1 - \frac{Z}{1 + Z + B^2 L_M^2} \right] \frac{\delta M}{M}$$

where  $Z = \Sigma_a \text{ Fuel} / \Sigma_a \text{ moderator}$

$B^2 =$  material buckling

$L_M^2 =$  diffusion length squared in the moderator,

and the data: (2)

$$Z = 3.45$$

$$L_M^2 = 12.02$$

$$B^2 = 0.00960$$



we see that:

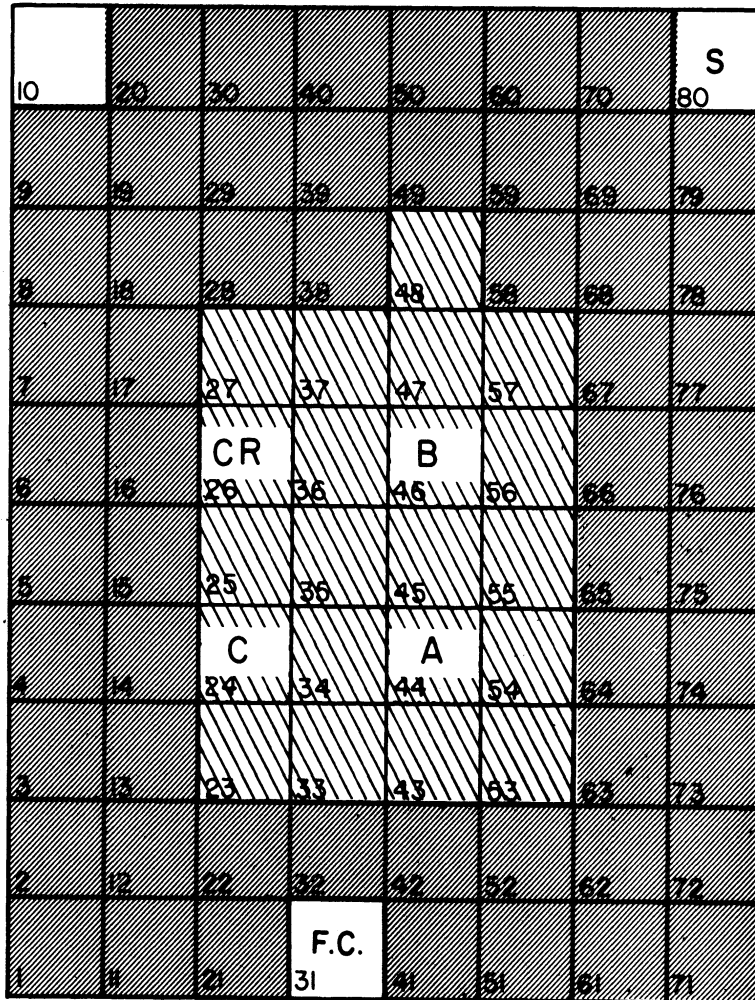
$$\frac{\delta k_{\text{eff}}}{k_{\text{eff}}} = 0.245 \frac{\delta M}{M}$$

Since  $M = 2539$  gms, and  $\frac{\delta k_{\text{eff}}}{k_{\text{eff}}} = 0.00406$ ,

$$\delta M = 42 \text{ gms.}$$

Thus critical mass = 2497 gms.

- A, B, C: Safety-Shim Rods (5 Plate Elements)
- CR: Control Rod (5 Plate Element)
- S: Po-Be Source
- F.C: Fission Chamber
-  Fuel Elements
-  Graphite Elements



LOADING 1a

Figure 1. Loading: 2539 gms.  
 Critical Mass: 2497 ± 5 gms.

## II. FLUX AND POWER MEASUREMENTS

The absolute flux values in the FNR were computed from measurements made with gold foils. The foil measurements were calibrated by comparison with foils irradiated in the standard pile at the Argonne National Laboratory. On the basis of these measurements, the power level was calculated and found to be  $0.58 \pm 0.052$  watts at a Log N reading of 0.021. This value of power was used to calibrate the reactor power level instrumentation.

The foils used were cut from 24 carat 0.001 inch thick, commercial gold foil. The average foil dimensions were 1.4 cm on a side and the average weight was 0.100 gm. Each foil was weighed in order to compensate for differences in size.

The foils were scotch-taped to the fuel elements, following the procedure used at Oak Ridge National Laboratory. This method, illustrated in Figure 2, made it possible to subdivide each fuel element into 4 power cells when making the power calculations.

The 0.411 mev gamma activity of the gold foils was counted in a well-type, scintillation counter (Radiation Counter Labs Type 23-A). All of the measured counts were corrected for decay and foil weight. Since two counting assemblies were used, all of the data was corrected to one of the assemblies, by using a standard Cs-137 source which was counted with both units. The measured activities are listed in Table I in counts per sec. per 100 mg.

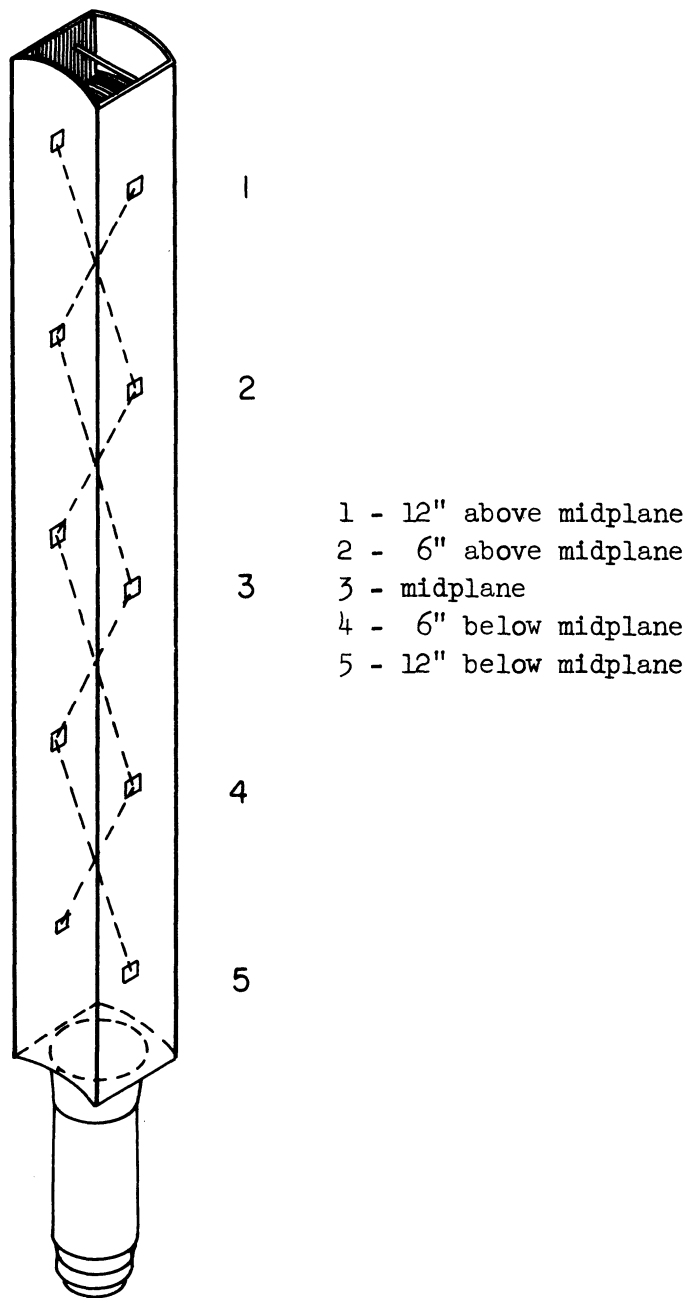


Figure 2. Fuel Element Showing Placement of Foils.

Because of the poisoning effects of the foils, the flux traverse for each fuel element required five separate irradiations. To standardize all of the data, a foil was placed in the same position in the core during each run and a correction factor for each set of measurements was obtained. The correlation of the activity of a foil from one irradiation to the activity of a similar foil from another irradiation assumes that gold foils exposed to a fixed neutron flux will activate linearly with time. As shown in Figure 3, this assumption is a good approximation for irradiation periods shorter than one hour. The longest exposure time for any set of foils was 30 minutes.

The thermal neutron population in the FNR was defined as being composed of all neutrons with energies below the cadmium cutoff energy of 0.4 ev. Thus, to measure the thermal flux, it was necessary to determine the cadmium ratio at representative points in the core.

$$\text{Cadmium Ratio} = \frac{\text{Activity of bare foil}}{\text{Activity of cadmium covered foil}} = \text{CR}$$

The irradiations of the foils used to determine cadmium ratios were made by mounting the foils on an aluminum frame which could be inserted between two fuel plates of any desired fuel element. This thin, paddle-like frame had 5 square holes in which the foils were taped. To place the foils in the frame in the same horizontal planes as those taped to the fuel elements, a stop was provided on the frame. The stop determined how far the frame would go down into the fuel element assembly.

Since it was felt that the cadmium ratio would vary slowly throughout the core, measurements were taken at the top,

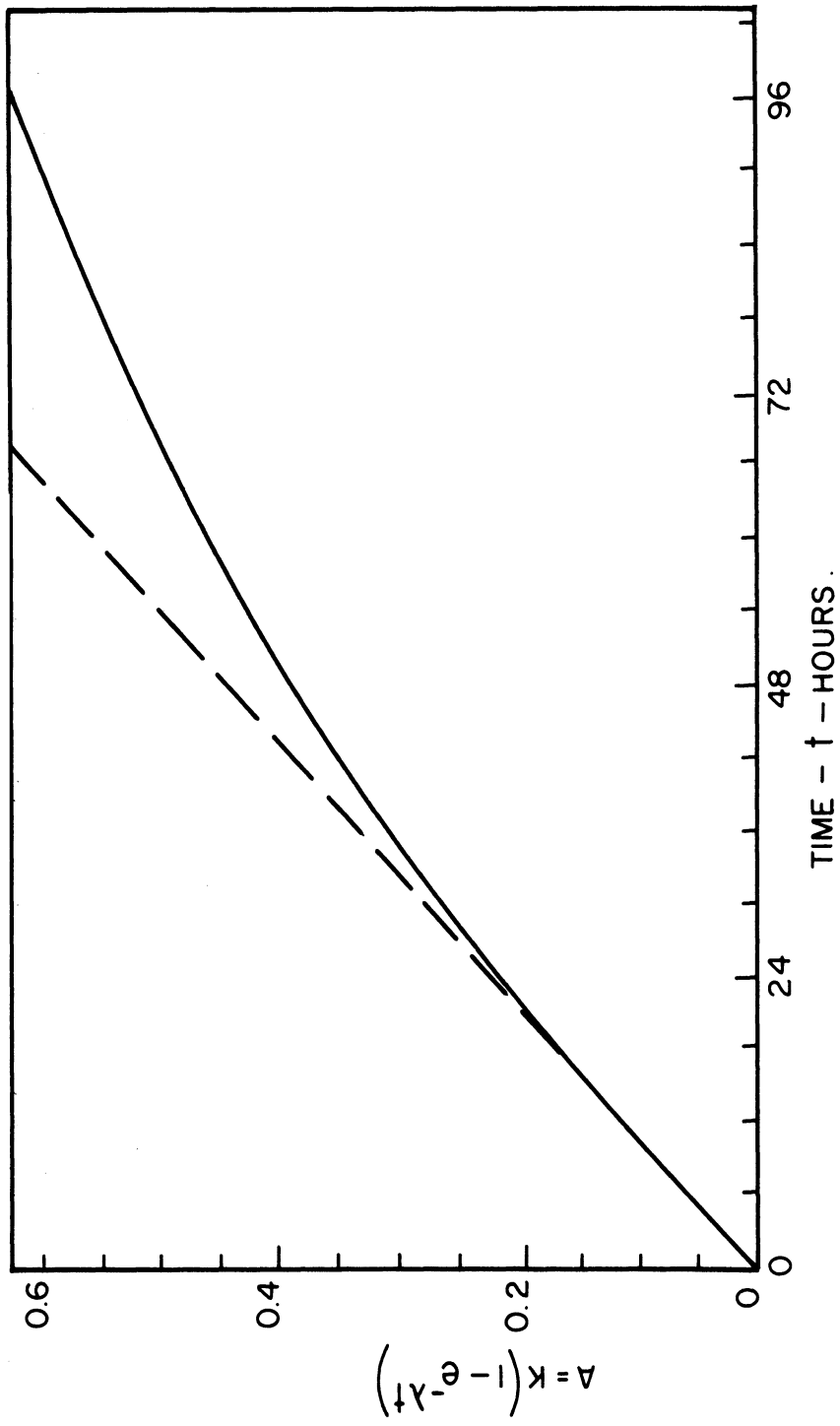


Figure 3. Activity Vs. Irradiation Time for Au<sup>198</sup> Normalized to 1.0. ( $T_{1/2} = 2.7$  days)



middle, and bottom planes only and the intermediate values were interpolated from plots of the measured data. These plots of cadmium ratios throughout the core are shown in Figures B-1, B-2, and B-3 in Appendix B. An investigation of the correlation between measurements made with taped-on foils and measurements made with the aluminum frame is being made. The results of this study will be reported in a future publication.

The flux at each measured point was calculated as follows:

$A_c^b$  = observed activity of bare foil including corrections for decay and foil weight

$A_s^b$  = Calculated saturated activity of bare foil

$A_s^{th}$  = Calculated saturated thermal activity

$$A_s^{th} = A_s^b - \frac{A_s^b}{CR}$$

$$CR = \text{Cadmium Ratio} = \frac{\text{Activity of bare foil}}{\text{Activity of cadmium covered foil}}$$

Because of the low flux levels in the ANL standard pile, the cadmium ratios are measured with indium. In the FNR, however, the use of indium leads to excessively high counting rates. Also the rapid decay of indium increases the possibility of error. Gold, with its lower cross section and longer half-life, proves to be more convenient.

The relationship between the cadmium ratio taken with indium foils and the cadmium ratio taken with gold foils was measured in the FNR and found to be:

$$\frac{CR_{Au}}{CR_{In}} = .95$$

Since no better information was available, this correction factor was applied to the cadmium ratios from ANL taken with indium to get corresponding ratios for gold.

$$(CR_{In}) \cdot .95 = CR_{Au}$$

Using this correction to determine the thermal saturated activities of the foils from Argonne and their corresponding flux values, the thermal flux in the FNR is:

$$\phi_{th}^{FNR} = A_S^{th} (FNR) \frac{\phi_{th}^{ANL}}{A_S^{th}}$$

$A_S^{th} (FNR)$  = saturated thermal activity measured in FNR

$\phi_{th}^{ANL}$  = flux values obtained from Argonne

$A_S^{th}$  = saturated thermal activity of Argonne foils.

Appendix C presents a typical calculation of the thermal flux at a point in the reactor. Figures B-8, B-9, and B-10 in Appendix B are graphs of the thermal flux in the individual elements. The thermal flux, cadmium ratios, saturated thermal activities, and saturated bare activities are tabulated in Table I. The saturated bare activities are the average of the two measured points on each side of the fuel elements. The measured (saturated) activities are listed in Table B-1 in Appendix B.

The power in the reactor was determined by dividing each fuel element into four power cells and then calculating the power produced in each cell. The sum of these individual power calculations gives the total integrated power of the reactor.

The following equation was used to calculate the power in each cell:

$$P = \phi \sum_f VE \text{ watts}$$

$$\sum_f = \text{macroscopic fission cross section (thermal) cm}^{-1}.$$

$$V = \text{volume of a power cell (cc)}$$

$$E = \text{energy per fission (watt-sec)}$$

$$\phi = \text{thermal neutron flux (n/cm}^2\text{sec)}$$

An average value of the thermal neutron flux for each power cell was obtained by cross-averaging the value of the flux at four points on the boundaries of the cell as shown in Figure 2. The computed power in each cell is shown in Table II.

In the preliminary calculations, a fission cross-section of 580 barns and an energy per fission of 193 mev. were used. These values give a power of 0.572 watts at a Log N reading of 0.021.

#### Corrections Applied to Preliminary Flux Values:

1. As mentioned previously, the Cd ratios obtained from ANL were measured with indium foils which had been irradiated in a graphite medium. The Cd ratio was measured in the FNR (water medium) with both gold and indium foils and it was determined that the two materials gave Cd ratios that differ by 5 per cent. When this correction was applied to the ANL values of Cd ratio, the assumption was made that Cd ratios measured in graphite are the same as Cd ratios measured in water. Further experimental work is planned to check the validity of this assumption.
2. The measurement of Cd ratio assumes that the Cd covers are completely "black" to thermal neutrons and completely "transparent"

to epithermal neutrons. These two conditions cannot exist simultaneously.<sup>(4)</sup> Therefore, a correction must be applied to the Cd ratios to account for the leakage of thermal neutrons through the cadmium and for the absorption of epithermal neutrons in the cadmium. Calculations, based on information in the literature<sup>(4)</sup>, give a correction factor of 2.5 per cent for 10 mil Cd covers in a region where the cadmium ratio is 2.8 (the average for FNR).

3. Because the foils were placed in the reactor before startup and not removed until after shutdown, the absolute flux values had to be corrected for the changing flux seen by the foils during startup and shutdown. This correction was made by graphically integrating the area under the Log N recorder trace and finding the ratio of the area under the startup and shutdown portions of the curve to the total area. (The area under the curve being directly proportional to the integrated flux). This correction had to be made only for the first (or standard) irradiation since all other irradiations were standardized to the first run and the activation of the foils is linear with respect to time (for small times). The startup correction on the standard run was 6 per cent.

4. One other correction has to be applied to the measured flux values in an effort to determine the absolute flux. This correction accounts for the depression of the flux caused by the insertion of the foils. At present very little information exists on the flux depression in heterogeneous uranium-water-aluminum media. However, on the basis of existing information it is estimated that the correction will not exceed 10 per cent. Since the magnitude of this correction has not been determined with any degree of certainty, it

has been included as an unknown error on the final value of flux. Experimental work is presently being conducted to determine this correction factor precisely.

Evaluation of Errors in Flux Measurements:

1. To minimize the error introduced in the counting of the foils, all of the foils were counted to a total count of more than 10,000, giving a probable error within 0.67 per cent. The effect of foil placement in the well counter was investigated and the associated error was found to be within the counting errors. Thus a probable error of  $\pm 0.67$  per cent due to counting has been applied to the final flux value.
2. The positioning of the foils on the fuel elements was done with an accuracy of approximately  $\pm 1$  mm. This error in placement gives an average flux error of  $\pm 1.5$  per cent, as determined from the vertical flux plots shown in **Figures B-8, B-9, B-10**.
3. The error introduced by incorrect placement of the foils used to measure the cadmium ratio was similarly determined from the cadmium ratio plots. A placement error of  $\pm 5$  mm. gives an average error in cadmium ratio of  $\pm 1.5$  per cent.
4. An error in the thermal flux will be introduced by extrapolation of cadmium ratios to unmeasured points. Since points were measured to give north-south and east-west plots of cadmium ratio on horizontal planes through the top, middle, and bottom of the core, it is felt that the extrapolated values obtained from the two different sets of curves are accurate within 5 per cent. The cadmium ratio varies relatively slowly from the top or bottom to the middle of the core (maximum 6.75 to 2.5 over 12 inches). Thus, the values

of cadmium ratio read from the vertical plots should be accurate within the limits set by the graphs ( $\pm 3$  per cent).

Errors No. 3 and 4 both apply to the cadmium ratio and must be added directly to give a total error in the value of the cadmium ratio of  $\pm 4.5$  per cent. However, since this combination of errors is independent of errors No. 1 and 2, which are also independent of each other, the total error may be calculated as the square root of the sum of the squares of the individual errors. This gives a total calculated error of  $\pm 4.85$  per cent. Therefore, the overall probable error in the absolute flux value is estimated as  $\pm 5$  per cent (neglecting flux depression), based on the Argonne National Laboratory's standard pile. Any error in the standard pile flux will cause a corresponding error in the absolute flux of the Ford Nuclear Reactor.

#### Corrections Applied to Preliminary Power Value:

1. In the preliminary power calculation the thermal fission cross section of U-235 was assumed to be 580 barns. This value must be corrected for non  $1/v$  dependence. The correction obtained from BNL-325 amounts to 1.73 per cent decrease in the cross section.
2. The contribution to the total power from fast fissions was neglected in the preliminary calculation. Measurements in a graphite thermal column indicated that at a cadmium ratio of 3.7, 93 per cent of all fissions occur below the cadmium cutoff.<sup>(3)</sup> Thus a fast fission correction amounting to + 7 per cent was added to the power value.
3. To obtain an average flux value for each of the power cells, the four flux values at the top and bottom edges of each cell were linearly cross-averaged.

Inspection of the flux plots shows that the maximum horizontal variation across a power cell is 1.5:1, and the maximum vertical variation from one horizontal plane to the adjacent plane is 3:1. Therefore, the procedure of linear averaging is probably good for these small variations, and the correction factor for this assumption will be considered to be zero or, at least, to be very much smaller than any of the other correction factors.

Evaluation of Errors in Power Calculation:

1. An error of  $\pm 1.4$  per cent in the value of the fission cross section is given in BNL-325. This error can be directly applied to the value of power calculated using the fission cross section of U-235.
2. The error in the assumed value of 193 mev. per fission is  $\pm 2.6$  per cent.<sup>(5)</sup> This error must also be applied to the power calculation.

The total error in the power calculation of the reactor for any given flux value is, by the square root of the sum of the squares of errors enumerated above,  $\pm 3$  per cent.

However, when stating the power level of the reactor reference should be made to the instrumentation channel used. In this calibration the Log N channel was used for reference. This channel was used rather than the Linear Level Channel because of the erratic behavior initially encountered in the Linear Level Compensated Ionization Chamber. The chart on this recorder can be read to  $\pm 2.5$  per cent. Therefore, the total error in the power level measurement of the reactor is estimated to be  $\pm 9$  per cent (including errors in flux measurement but again excluding flux depression in the foils).

The reactor power will be checked against the X-10 standard pile at Oak Ridge, and, in an effort to reduce the errors which are caused by uncertainties in such quantities as fast fission factor and fission cross section, a method of calibration described in the literature<sup>(6)</sup> may also be utilized. A final check of the power at levels of 100 kw or greater will be made, using calorimetric techniques.



TABLE I

Saturated Activities, Cadmium Ratio and Thermal Flux  
(Power = 0.58 watts)

<u>Position</u>	<u><math>A_S^b \times 10^{-4}</math></u>	<u>Cd Ratio</u>	<u><math>A_S^{th} \times 10^{-4}</math></u>	<u><math>nv^{th} \times 10^{-6}</math></u>	
23	1	3.79	5.11	3.05	2.87
	2	6.74	2.80*	4.33	4.07
	3	8.08	2.46	4.78	4.49
	4	6.25	2.68*	3.92	3.68
	5	3.54	3.23	2.45	2.30
33	1	4.17	4.45*	3.23	3.03
	2	7.99	2.58*	4.89	4.59
	3	9.26	2.36*	5.34	5.01
	4	7.21	2.72*	4.56	4.28
	5	4.50	3.5*	3.22	3.02
43	1	3.95	5.83	3.27	3.07
	2	8.03	3.07*	5.41	5.09
	3	9.68	2.51	5.88	5.53
	4	7.52	2.54*	4.56	4.28
	5	4.63	2.84	3.01	2.83
53	1	3.81	6.84*	3.25	3.05
	2	7.09	3.60*	5.12	4.81
	3	8.71	2.88*	5.67	5.34
	4	6.95	2.61*	4.29	4.03
	5	3.84	2.59*	2.36	2.21
24	1	2.68	4.35*	2.06	1.94
	2	9.52	2.53*	5.76	5.41
	3	11.20	2.25*	6.23	5.85
	4	8.30	2.53*	5.02	4.72
	5	5.00	3.31*	3.49	3.28

\* Interpolated value from graphs

Position	$A_S^b \times 10^{-4}$	Cd Ratio	$A_S^{th} \times 10^{-4}$	$nv_{th} \times 10^{-6}$	
34	1	3.76	4.08	2.84	2.67
	2	11.36	2.46*	6.74	6.33
	3	13.53	2.34	7.77	7.29
	4	10.65	2.81*	6.86	6.44
	5	5.92	3.70	4.31	4.05
44	1	4.18	4.52*	3.26	3.06
	2	11.93	2.81*	7.69	7.22
	3	14.31	2.50*	8.59	8.07
	4	10.53	2.73*	6.68	6.27
	5	6.10	3.46*	4.34	4.08
54	1	3.91	4.78	3.09	2.91
	2	10.48	3.00*	7.09	6.66
	3	11.74	2.83	7.23	6.79
	4	9.30	2.70*	5.86	5.50
	5	4.96	3.07	3.35	3.14
25	1	5.00	4.01	3.74	3.53
	2	8.91	2.52*	5.37	5.05
	3	10.55	2.16	5.69	5.34
	4	8.49	2.53*	5.14	4.83
	5	4.86	3.35	3.40	3.20
35	1	5.91	5.01	4.73	4.44
	2	11.13	3.00*	7.54	7.08
	3	11.47	2.58	7.02	6.59
	4	10.38	2.87*	6.76	6.35
	5	6.04	3.62	4.38	4.12
45	1	5.74	4.35	4.42	4.15
	2	11.85	2.82*	7.65	7.18

\* Interpolated value from graphs

<u>Position</u>		<u><math>A_S^b \times 10^{-4}</math></u>	<u>Cd Ratio</u>	<u><math>A_S^{th} \times 10^{-4}</math></u>	<u><math>nv_{th} \times 10^{-6}</math></u>
45	3	12.00	2.48	7.16	6.73
	4	11.31	2.81*	7.28	6.84
	5	6.55	3.69	4.48	4.20
55	1	5.07	4.75*	4.00	3.76
	2	10.69	2.68*	6.69	6.29
	3	10.51	2.38*	6.10	5.73
	4	10.19	2.64*	6.33	5.94
	5	5.74	3.30*	4.00	3.76
26	1	3.67	4.15*	2.79	2.62
	2	8.59	2.47*	5.11	4.80
	3	10.55	2.22*	5.80	5.45
	4	9.99	2.51*	6.02	5.65
	5	5.33	3.30*	3.72	3.49
36	1	4.66	4.15	3.53	3.32
	2	10.93	2.57*	6.68	6.28
	3	13.22	2.37	7.67	7.20
	4	11.34	2.72*	7.17	6.73
	5	6.45	2.52	4.57	4.29
46	1	4.73	4.40*	3.66	3.43
	2	12.18	2.72*	7.70	7.23
	3	14.37	2.45*	8.50	7.99
	4	11.55	2.73*	7.33	6.88
	5	7.07	3.48*	5.04	4.74
56	1	4.64	4.49	3.61	3.39
	2	10.92	2.60*	6.72	6.31
	3	12.01	2.30	6.79	6.37

\* Interpolated value from graphs

<u>Position</u>		<u><math>A_S^b \times 10^{-4}</math></u>	<u>Cd Ratio</u>	<u><math>A_S^{th} \times 10^{-4}</math></u>	<u><math>nv_{th} \times 10^{-6}</math></u>
56	4	9.20	2.61*	5.68	5.33
	5	5.74	3.25	3.99	3.74
27	1	3.34	4.57	2.60	2.45
	2	6.98	2.73*	4.43	4.16
	3	8.54	2.35	4.90	4.60
	4	6.86	2.50*	4.11	3.86
	5	3.70	3.09	2.50	2.35
37	1	4.16	5.14*	3.35	3.15
	2	8.47	2.82*	5.46	5.13
	3	9.78	2.47*	5.82	5.47
	4	8.10	2.60*	4.98	4.68
	5	5.04	3.08*	3.40	3.19
47	1	5.30	5.14	4.27	4.01
	2	8.86	2.95*	5.86	5.50
	3	10.27	2.47	6.08	5.71
	4	8.12	2.49*	4.86	4.56
	5	5.25	2.91	3.45	3.24
57	1	4.36	6.77	3.72	3.49
	2	8.05	3.80*	5.93	5.57
	3	9.44	2.49	5.64	5.30
	4	7.08	2.37*	4.09	3.85
	5	4.03	2.69	2.53	2.37
48	1	3.85	5.88*	3.19	3.00
	2	6.38	3.38*	4.49	4.22
	3	7.85	2.49*	4.69	4.41
	4	6.63	2.18*	3.59	3.37
	5	3.45	2.10*	1.81	1.70

\* Interpolated value from graphs

TABLE II

## Power Output per Cell

<u>Position</u>	<u>Element and Power Cell</u>	<u><math>\phi_{th}^{(nv)} \times 10^{-6}</math></u>	<u>Grams Fuel</u>	<u>Power (watts)</u>
33	1-1	3.93	35	.00632
	2	4.04	35	.00649
	3	4.02	35	.00647
	4	3.11	35	.00500
25	2-1	4.37	35	.007031
	2	5.15	35	.00828
	3	5.05	35	.00813
	4	4.11	35	.00661
53	3-1	3.94	35	.00634
	2	5.07	35	.00816
	3	4.63	35	.00745
	4	3.40	35	.00547
23	4-1	3.32	35	.00534
	2	4.20	35	.00675
	3	4.05	35	.00652
	4	3.03	35	.00487
43	5-1	3.79	35	.006096
	2	5.26	35	.00845
	3	4.86	35	.00782
	4	3.58	35	.00576
34	6-1	4.66	35.25	.00755
	2	6.61	35.25	.01070
	3	6.84	35.25	.01110
	4	5.35	35.25	.00867

<u>Position</u>	<u>Element and Power Cell</u>	<u><math>\phi_{th}(nv) \times 10^{-6}</math></u>	<u>Grams Fuel</u>	<u>Power (watts)</u>
45	7-1	5.78	35.25	.00936
	2	6.86	35.25	.01111
	3	6.70	35.25	.01086
	4	5.76	35.25	.00933
36	8-1	4.89	35.25	.00793
	2	6.60	35.25	.01070
	3	6.92	35.25	.01120
	4	5.61	35.25	.00909
37	9-1	4.27	35.25	.00693
	2	5.19	35.25	.00841
	3	5.00	35.25	.00809
	4	3.97	35.25	.00643
54	10-1	4.84	35.25	.00784
	2	6.60	35.25	.01070
	3	6.10	35.25	.00988
	4	4.35	35.25	.00706
55	11-1	5.13	35.25	.00831
	2	5.83	35.25	.00944
	3	5.76	35.25	.00933
	4	4.92	35.25	.00798
47	12-1	4.79	35	.00771
	2	5.54	35	.00892
	3	5.04	35	.00810
	4	3.91	35	.00629
56	13-1	4.99	35	.00802
	2	6.20	35	.00998
	3	5.81	35	.00935
	4	4.60	35	.00739

<u>Position</u>	<u>Element and Power Cell</u>	<u><math>\phi_{th} (nv) \times 10^{-6}</math></u>	<u>Grams Fuel</u>	<u>Power (watts)</u>
57	14-1	4.66	35	.007497
	2	5.44	35	.00875
	3	4.46	35	.00717
	4	3.17	35	.00501
27	15-1	3.38	35	.00544
	2	4.34	35	.00698
	3	4.19	35	.00675
	4	3.15	35	.00507
48	16-1	3.64	35	.00585
	2	4.34	35	.00698
	3	3.84	35	.00618
	4	2.49	35	.00401
35	19-1	5.77	35.25	.0094
	2	6.69	35.25	.0108
	3	6.47	35.25	.0105
	4	5.30	35.25	.0086
26	CR-1	3.82	9.3	.00171
	2	5.00	9.3	.00223
	3	5.47	9.3	.00244
	4	4.69	9.3	.00210
44	A-1	5.29	9.3	.00236
	2	7.54	9.3	.00337
	3	7.13	9.3	.00319
	4	5.24	9.3	.00234
46	B-1	5.50	9.3	.00246
	2	7.48	9.3	.00334
	3	7.40	9.3	.00331
	4	5.89	9.3	.00263

<u>Position</u>	<u>Element and Power Cell</u>	<u><math>\phi_{th}(nv) \times 10^{-6}</math></u>	<u>Grams Fuel</u>	<u>Power (watts)</u>
24	C-1	3.87	9.3	.00173
	2	5.52	9.3	.00247
	3	5.23	9.3	.00234
	4	4.08	9.3	.00182



### III. ROD CALIBRATIONS

#### Control Rod

The stainless steel control rod was calibrated by the "pile-period" method using the inhour equation. This method is described in the literature.<sup>(7,8)</sup> During the experiments, it was found necessary to remove the Po-Be source from the reactor to get reproducible results. The presence of the source seemed to affect the measurements when the control rod was half-inserted. A similar effect has been observed on the Pennsylvania State University reactor.

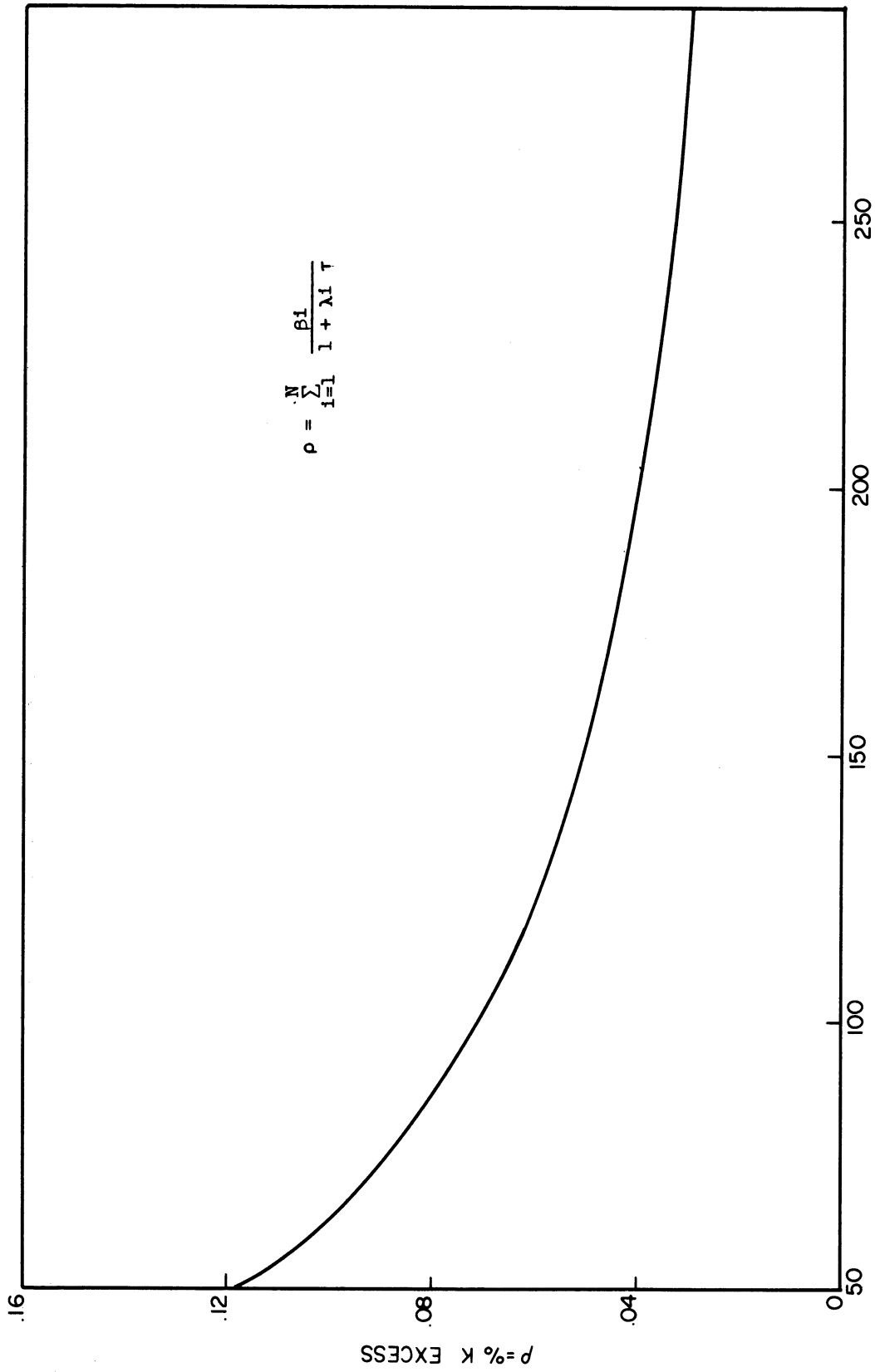
The differential rod worth curve calculated from the experimental data by using the inhour equation (Figure 4) is shown in Figure 5. This curve was graphically integrated to give rod worth as a function of position (Figure 6). The overall worth of the control rod in this configuration is 0.292 percent.

#### Safety-Shim Rods

The three safety-shim rods were calibrated for their first 4 1/2" of insertion (Figure 7) by compensating for a small insertion of a particular rod by withdrawal of the control rod to maintain criticality. The control rod calibration curve gives the change in reactivity caused by the shim rod movement. No correction was made for the shading effects of one rod upon another.

The positions of the rods are read on scales attached directly to the rod actuator housing. The shim-rod scales can be read to 1/100 inch while the control-rod scale can be read to 1/32 inch.

The reactor power level during the above experiments was approximately 2.5 watts.



$\tau$  = REACTOR PERIOD (sec)

Figure 4. Reactor Period Vs. Positive  $K_{ex}$

TABLE III  
CONTROL ROD WORTH DATA

Exp. #	Reading	R1(in.)	R2(in.)	Doubling Time (sec.)	Period (sec.)	Percent $\Delta k/k/\text{inch}$
34	1	30 1/16	26 5/16	76.9	111	0.0172
	2	27 13/16	24 25/32	90.0	130	0.0187
	3	26 3/16	21 31/32	53.7	77.5	0.0201
	4	23 29/32	20 27/32	85.5	123.4	0.0193
	5	21 7/16	17 9/16	86.4	124.7	0.0152
	6	17 25/32	14 13/32	206.0	297.5	0.0089
35	1	35 13/16	31 1/16	190.0	274	0.0062
	2	32 11/16	28 21/32	106.5	153.8	0.0123
	3	29 3/8	26	83.3	119.7	0.0177
	4	27 3/16	24 3/4	113.2	163.4	0.0194
	5	26	23 1/2	105.1	151.8	0.0200
	6	24 23/32	21 3/4	89.4	129.0	0.0193
	7	22 1/8	18 29/32	95.9	138.2	0.0167
	8	20 3/8	16 1/8	97.7	140.5	0.0125
	9	17 13/16	14 5/16	197.7	285.5	0.0086

Note: Control Rod Scale Readings:

100 percent out = 11 13/16"

Completely in = 35 13/16"

Total Travel = 24"

R1: Initial Control Rod Position

R2: Final Control Rod Position

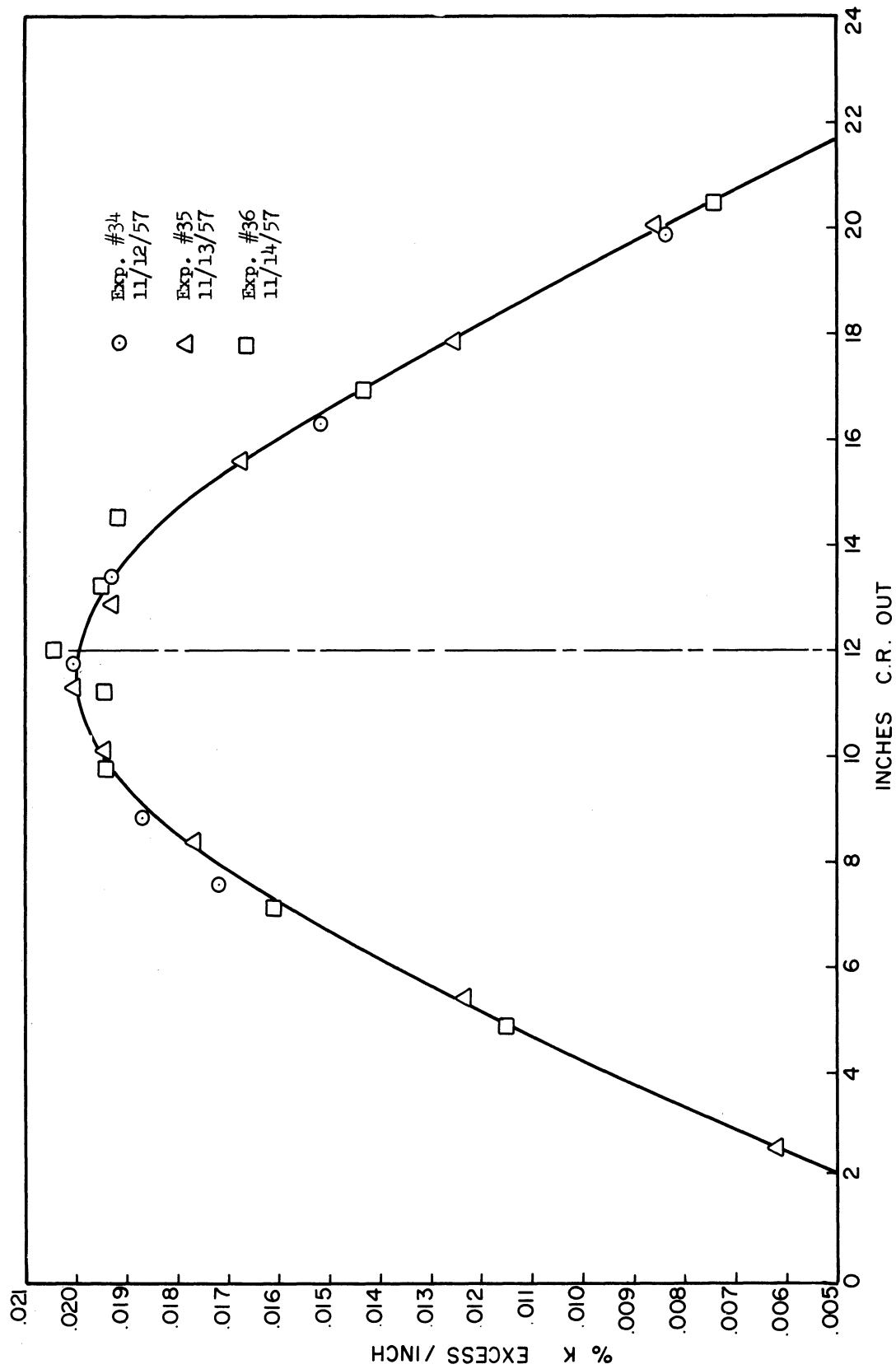


Figure 5. Control Rod Calibration.

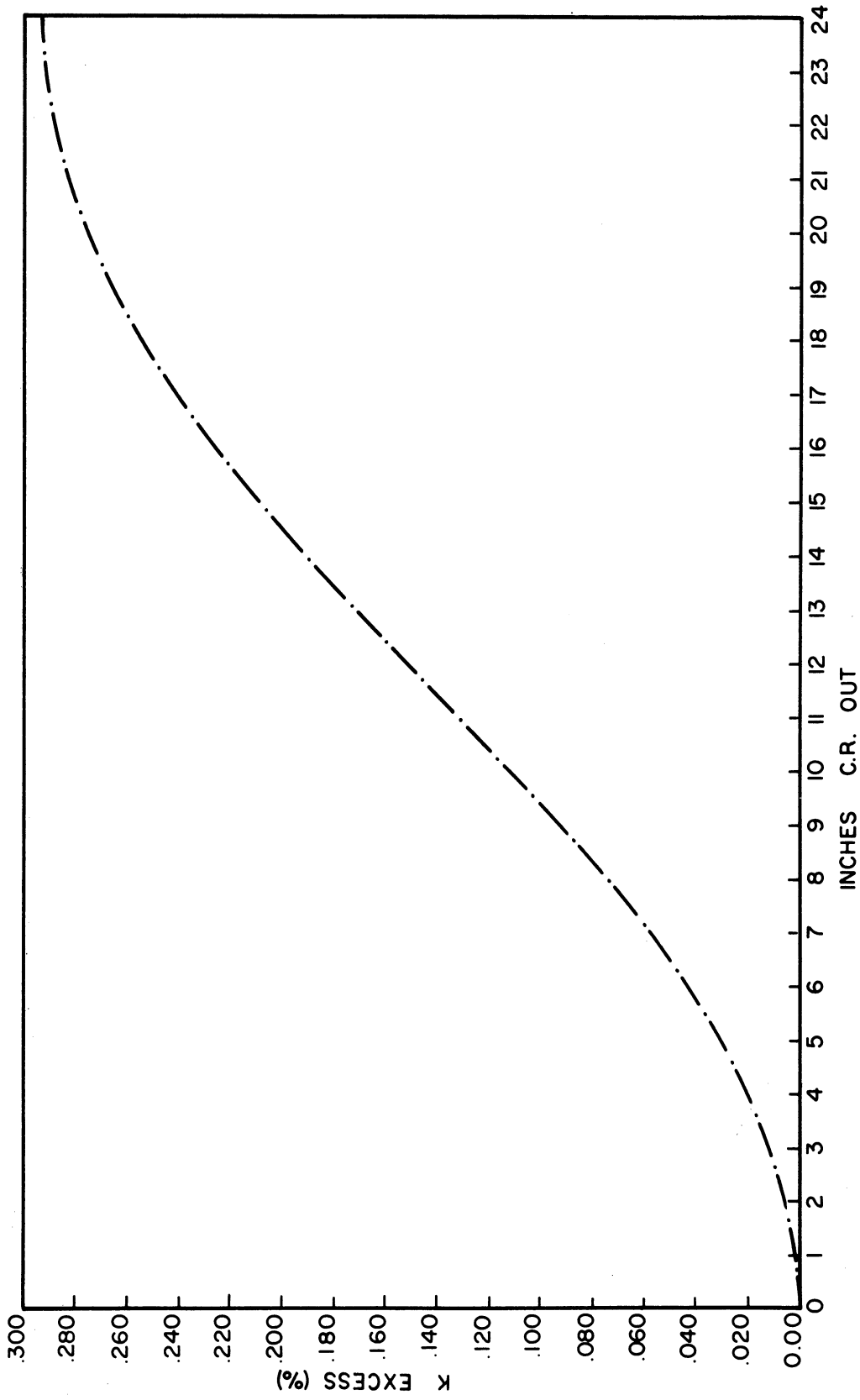


Figure 6. Control Rod Calibration-Loading 1a.

TABLE IV

SAFETY-SHIM ROD CALIBRATION

Exp. #	Run#	Control Rod Position(in.)	A(in.)	B(in.)	C(in.)
38	1	32 27/32	11.99	13.73	13.68
	2	29 30/32	12.82	"	"
	3	28 9/32	13.30	"	"
	4	26 19/32	13.80	"	"
	5	25	14.24	"	"
	6	22 3/32	14.72	"	"
	7	20 7/32	15.29	"	"
	8	16 12/32	15.75	"	"
	9	24 3/4	15.75	12.00	12.00
	10	20 5/32	16.42	"	"
	11	15 1/32	16.90	"	"
39a	1	32 9/16	13.90	12.00	13.72
	2	29 11/16	"	12.75	"
	3	27 7/8	"	13.12	"
	4	26 1/8	"	13.70	"
	5	24 1/8	"	14.17	"
	6	21 7/8	"	14.65	"
	7	18 1/8	"	15.12	"
	8	26 7/8	12.02	15.07	12.00
	9	23 1/8	"	15.66	"
	10	19 11/16	"	16.12	"
	11	12 23/32	"	16.45	"
	12	32 7/8	13.55	13.55	12.00
	13	31 5/16	"	"	12.65
	14	30 1/16	"	"	13.20
	15	28 7/8	"	"	13.66
	16	27 23/32	"	"	14.15
	17	26 5/8	"	"	14.55
	18	25 3/8	"	"	15.02
	19	23 7/8	"	"	15.52
	20	22 7/16	"	"	15.97
	21	20 5/16	"	"	16.50
	22	16 9/16	"	"	17.10
	23	13 1/16	"	"	17.35

Note: Shim Rod Scale Readings:

Shim Rod 100 percent out = 12.00"

Shim Rod completely in = 36.00"

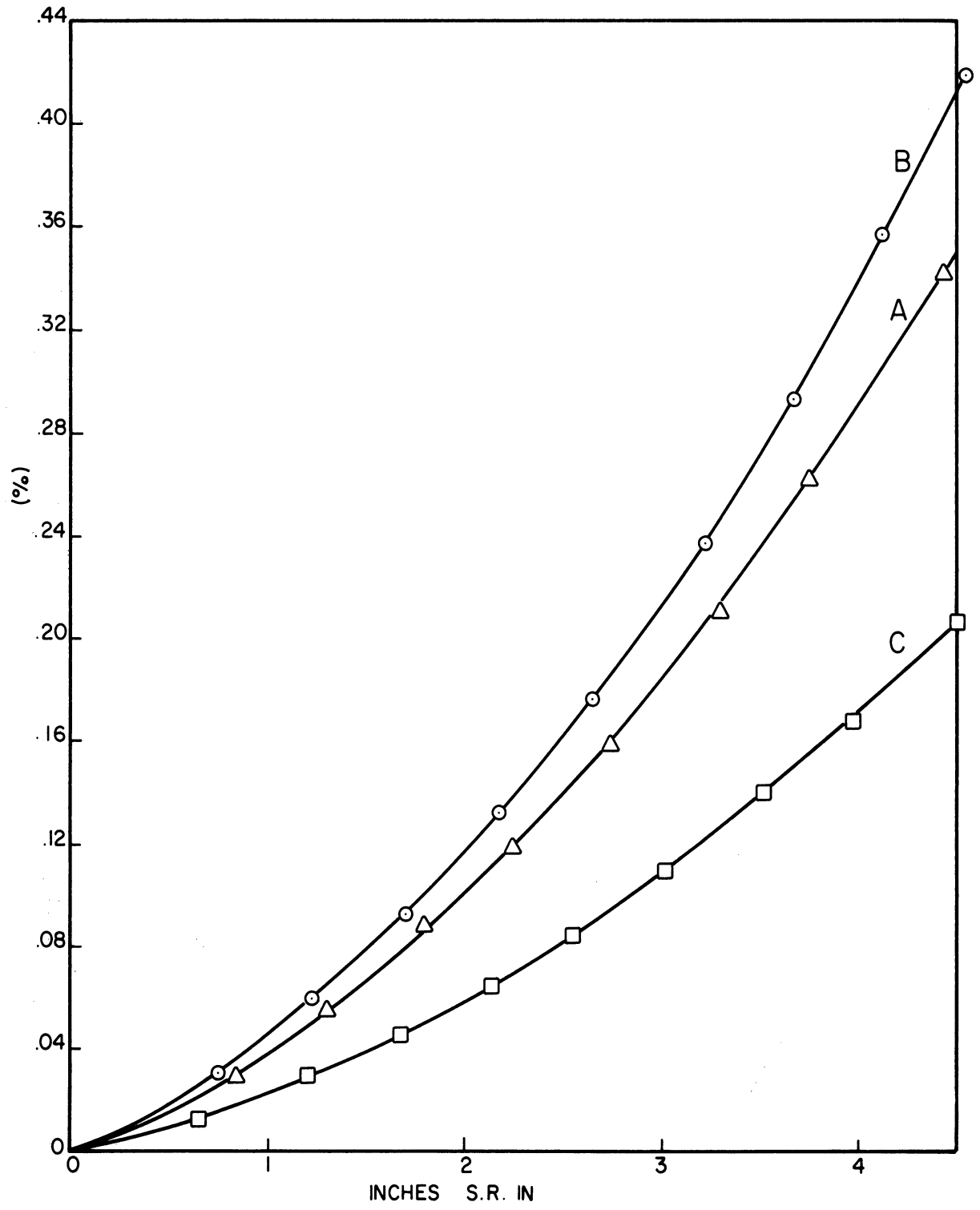


Figure 7. Safety Rod Calibration-Loading 1a.

Since core loading 1a contains only about 0.4 percent excess reactivity, it was not possible to calibrate the worth of the shim rods over their entire length by the above method. Therefore a rod-drop method was employed to measure the overall worth of each rod. With the power level stabilized at 100 kw a rod was dropped from its uppermost position by lowering its magnet current below the holding point. The traces on the linear level and log-count-rate recorders were observed, and the positions of the traces, 14 seconds after the drop, were marked. The curve in Figure 8 shows the relationship between the relative power and a step insertion of  $-K$  dollars of reactivity at time zero. This curve was plotted using data from the Reactor Handbook.<sup>(9)</sup>

Table V gives the results of three drops of each rod. The rod worths obtained using the average values of relative powers are:

A: 3.53 percent  $\Delta k/k$

B: 3.77 percent  $\Delta k/k$

C: 1.94 percent  $\Delta k/k$

The accuracy associated with this method is estimated as  $\pm 10$  percent.



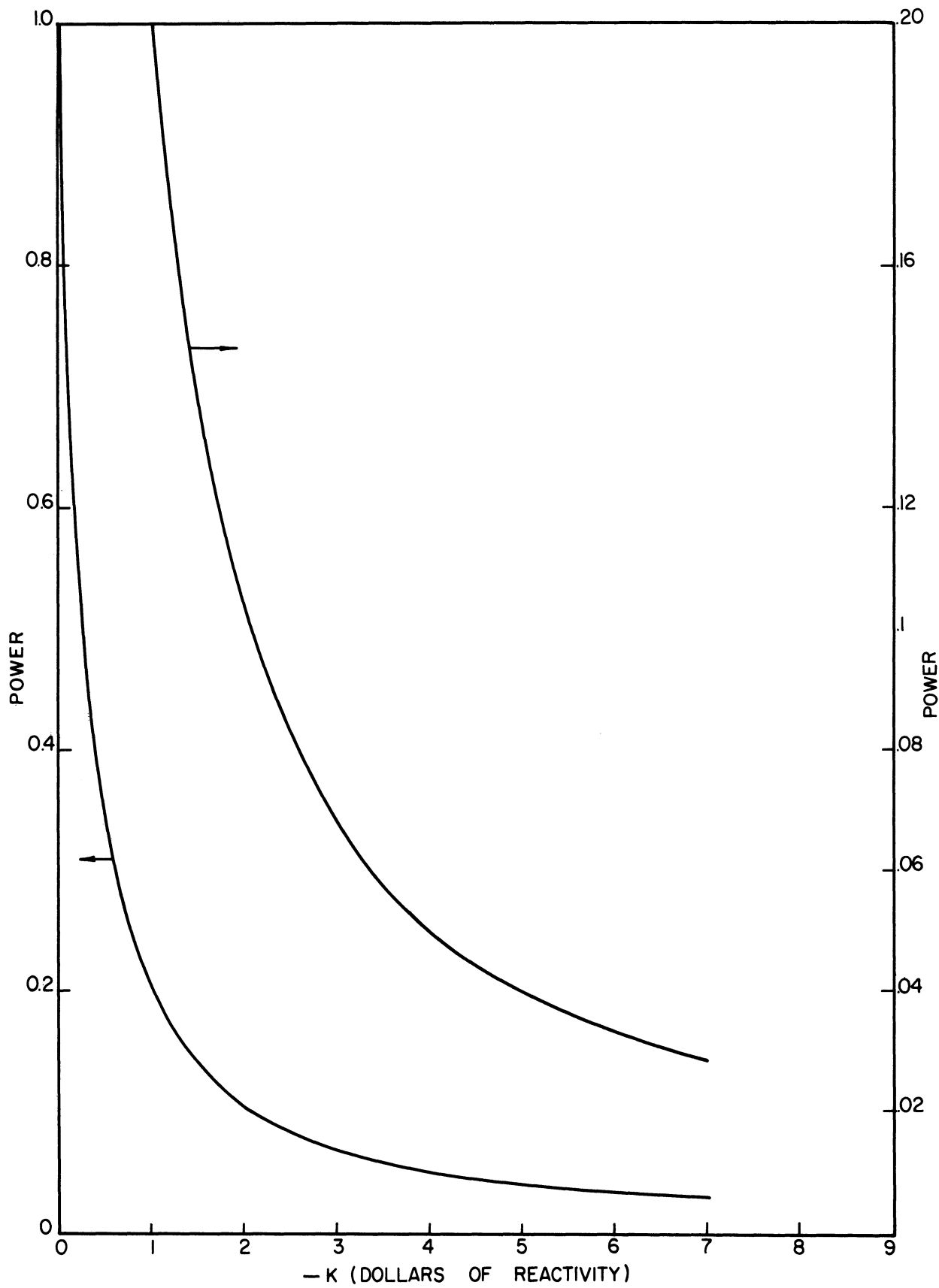


Figure 8. Relative Power 14 Seconds After Step Decrease in Reactivity of K Dollars.

TABLE V

Relative Power 14 seconds After Rod Drop

Exp. #	Rod A		Rod B		Rod C	
	1*	2	1	2	1	2
96	.0435	.0562	.0397	.0428	.0800	.0889
97	.0425	.0354	.0406	.0362	.0770	.0775
98	.0428	.0426	.0413	.0389	.0880	.0728
Average	.0438		.0398		.0807	

\* Numbers 1 and 2 refer to data from the Linear Level and Log-Count-Rate channels, respectively.

#### IV. TEMPERATURE COEFFICIENT

The temperature coefficient of the FNR was measured over a range well above and below the nominal operating temperature of 90°F and found to be  $-5.5 \times 10^{-5} \Delta k/k$  per degree F. @ 90°. The pool water was heated by an external heat source rather than from the reactor to minimize the buildup of fission product radioactivity in the fuel. Heating was accomplished by feeding steam into the tube side of the heat exchanger while circulating pool water through the shell side.

After the pool had reached an equilibrium temperature of approximately 120°F., the reactor was brought to a power level of approximately 5.5 watts. The steam was turned off and cooling water returned to the secondary side of the heat exchanger. The reactor was then operated on automatic control while the pool was cooled. At periodic intervals during the cooling the reactor was put on manual control and stabilized on an infinite period. The primary pump circulated pool water continuously while the secondary pump was shut off during each measurement period. The temperatures in the core and the setting of the control rod were then recorded. A curve of reactivity added to maintain criticality vs. temperature is shown in Figure 9.

The average core temperature was measured using six thermocouples placed as shown in Figure 10. The data from these thermocouples are tabulated in Table VI.

Concurrently with the temperature coefficient experiment, data were taken to determine the stratification of the pool water during cooling. This was accomplished by suspending thermocouples from the

TABLE VI

## TEMPERATURE COEFFICIENT DATA

(LOG N = 0.1; POWER LEVEL = 2.7 Watts)

## Temperatures (°F)

Time	Lattice Position	Top**		Middle**		Bottom**		Control Rod Position (In.)
		27	34	57	35	55	36	
1142	118	119.5	113.5	120	118.5	115	11-13/16	
1150	116	120	114	120.5	120	115.5	12	
1211	121	121	115	122.5	120.5	117		
1222	107.5	121	114	122.5	120	116.5	15	
1245	110.5	116	114.5	112	115	111.5	18-15/32	
1305	107	113.5	110	110	112	107	19-31/32	
1358	99	105	102	102	104	100.5	21-5/8	
1426	97	104.5	101	100.5	102	99	22-5/8	
1452	92	100.0	86	96	95	93	24-3/8	
1518	86	94	90.5	94	92	90.5	25-7/8	
1550	86.5	89	86	95	85	83	27-1/8	
1627	83	86.5	82	85	84	80.5	27-25/32	
1635	84	86.5	83	85	88	81.5	27-27/32	
1716	77.5	80*	77	80	78	74	29-19/32	
1749	69	75	69	69	71	67	32-1/4	
1803	70	75	69	68	72	68	31-1/2	
1823	63	72	67	74	70	64.5	33-1/8	
1845	65	64	64	67	66	65	25-1/4 <sup>+</sup>	
1852	67	66	64	68	66	61.5	25	

\*Very erratic

+"C" rod shimmed

\*\*These positions are the top, middle, and bottom of the particular fuel elements in these lattice positions.

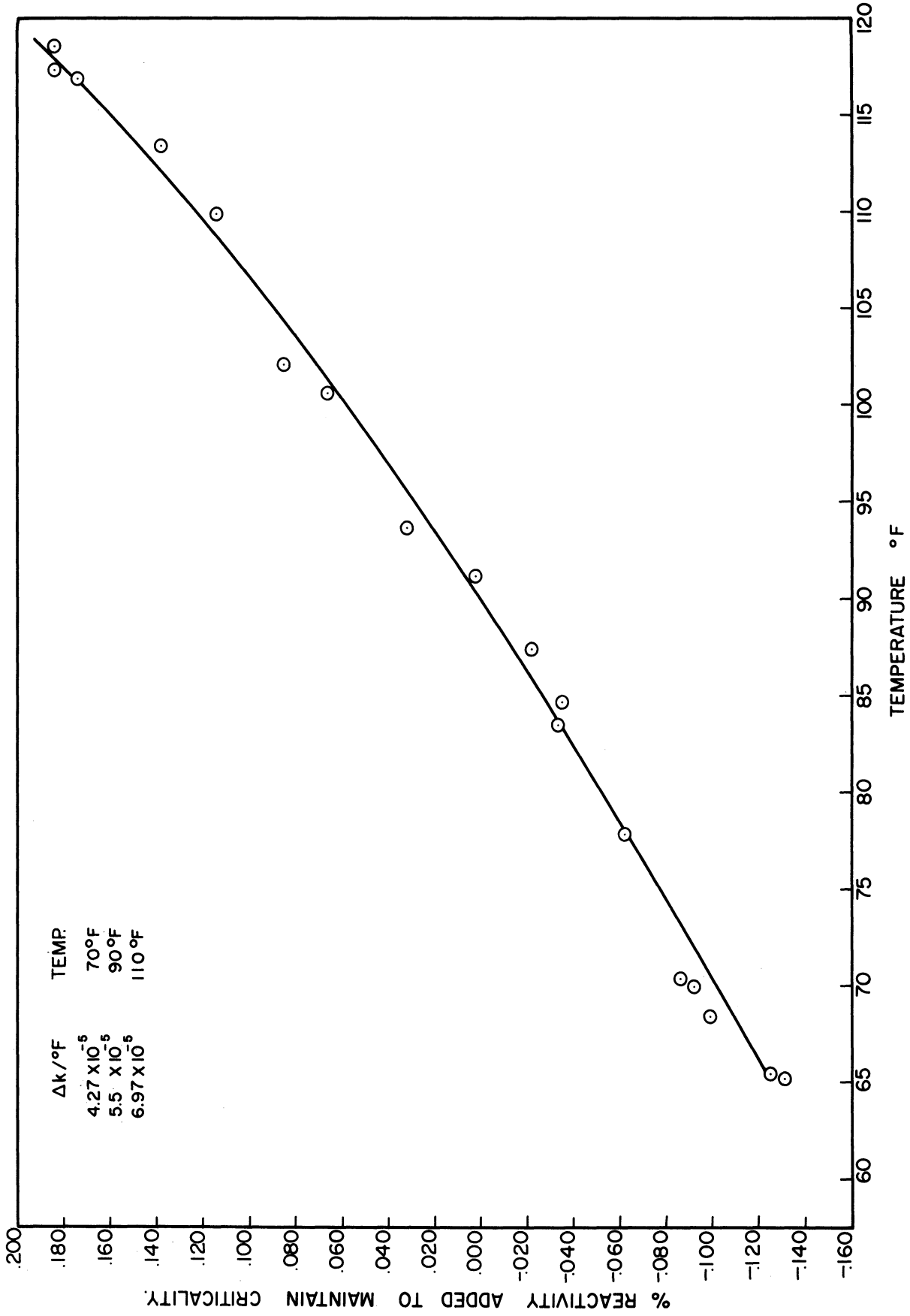
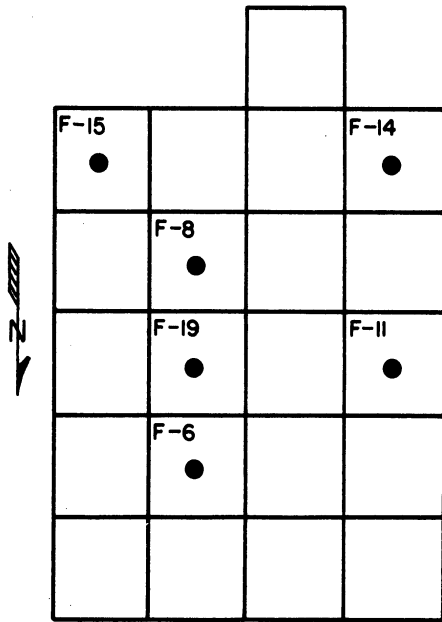


Figure 9. Temperature Coefficient of FNR.

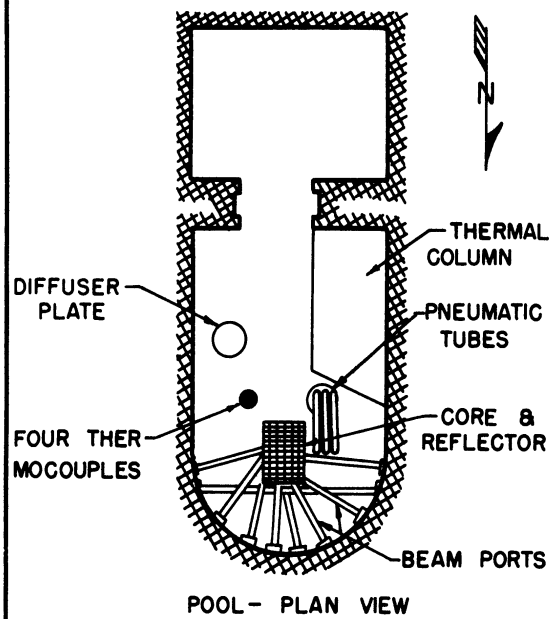
LATERAL DISTRIBUTION OF THERMOCOUPLES WITHIN THE CORE.



CORE-PLAN VIEW

FIGURE - 10a

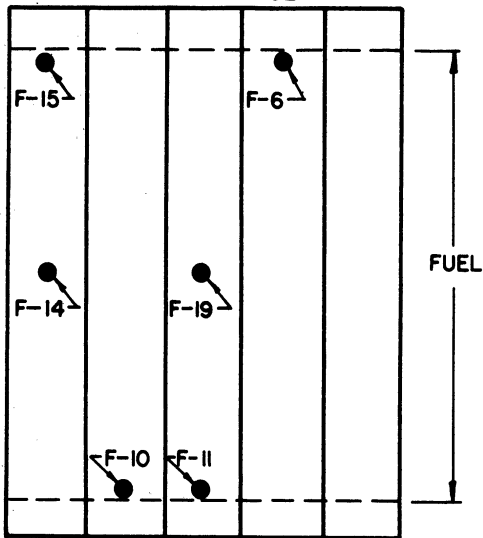
LOCATION OF THERMOCOUPLES USED TO MEASURE STRATIFICATION.



POOL - PLAN VIEW

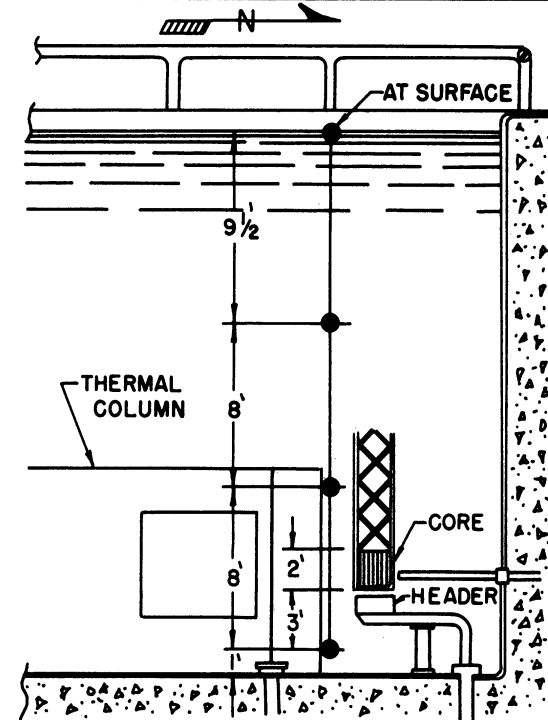
FIGURE - 10b

CORE - EAST FACE



VERTICAL DISTRIBUTION OF THERMOCOUPLES WITHIN THE CORE.

FIGURE - 10c



- POOL - SECTION -  
VERTICAL LOCATION OF STRATIFICATION THERMOCOUPLES.

FIGURE - 10d

bridge at known distances above the pool floor. The data are presented graphically in Figure 11, along with a plot of the overall core temperature. These plots show that the upper two-thirds of the pool are relatively stagnant at the low flow rate used ( $\sim 400$  gpm), and that most of the water drawn through the core comes from the lower third of the pool.

This stratification tends to minimize the radiation hazard at the pool surface from induced nitrogen activity in the water. The stratification effect, observed in this experiment, arises from two factors. First, the pool water has been heated and that portion which is drawn through the core to the heat exchanger and returned to the pool is at a lower temperature than the main body (upper two-thirds) of pool water. Secondly, the inlet to the pool for water return from the heat exchanger is covered with a diffuser plate which directs the flow across the bottom of the pool. The second of these two factors will function independent of water temperature, while the first is a temperature dependent effect.

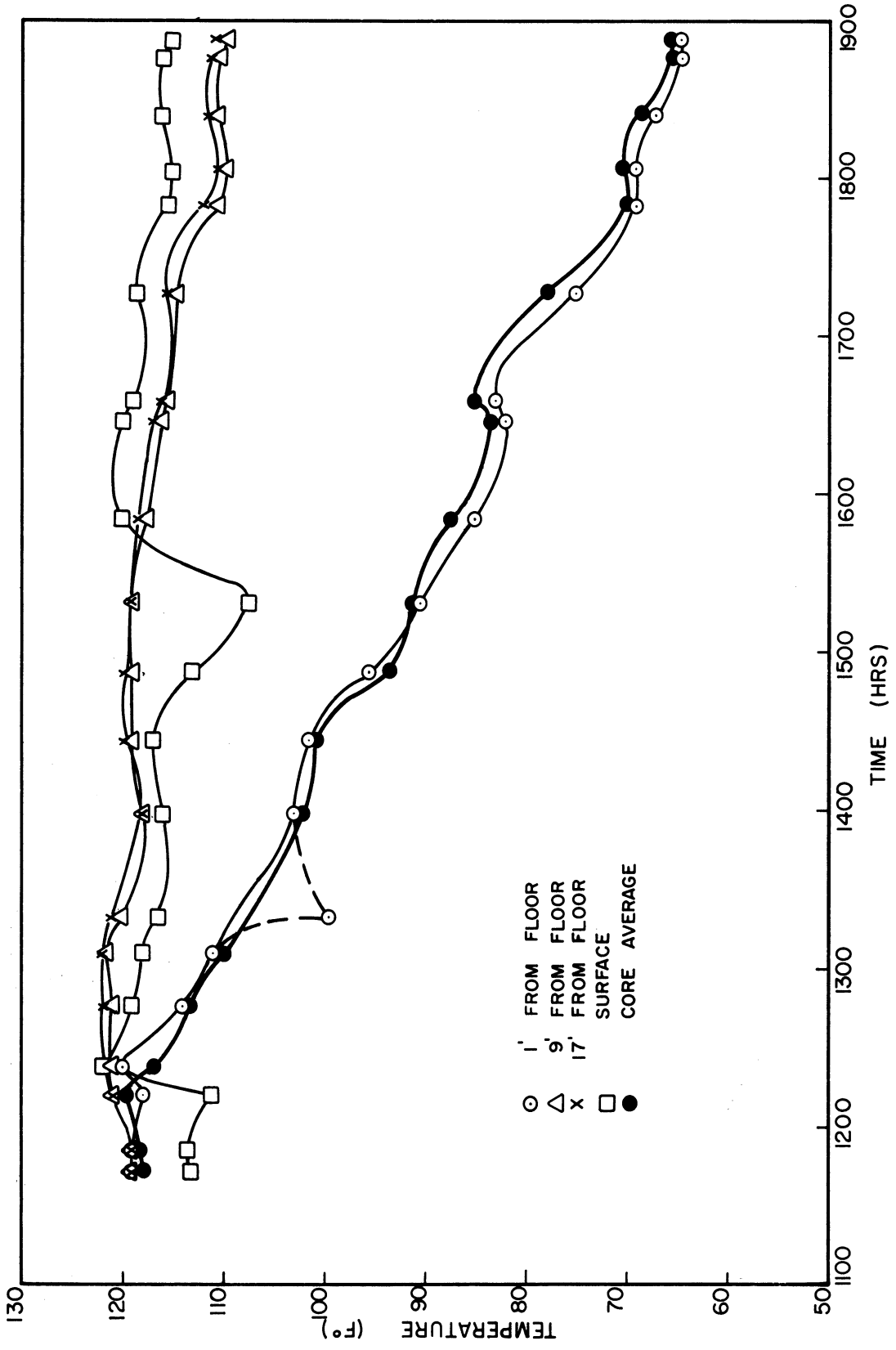


Figure 11. Pool Water Temperatures During Temperature Coefficient Measurement.



## V. Reactivity Effects

The effects of voiding beam tubes, of inserting cadmium absorbers in the pneumatic tubes, and of placing a 1/8" Boral sheet (24" x 24") adjacent to certain faces of the reactor was measured by observing the resultant changes in control rod position to maintain criticality. The reactor was moved to the thermal column position and the effect on criticality was measured. Table VII gives the results of these investigations.

TABLE VII

Reactivity Worth

<u>Action</u>	<u>Reactivity (%)</u>
Voiding Ports	
J (8") . . . . .	-0.009
G (8") . . . . .	-0.004
B (Thru port) . . . . .	-0.003
C (Thru port) . . . . .	-0.001
F (6") . . . . .	-0.001
A (6") . . . . .	-0.009
D (6") . . . . .	-0.001
E (6") . . . . .	0
H (6") . . . . .	-0.0015
I (6") . . . . .	-0.001
Cd in all 4 pneumatic tubes (about 4 gm in each)	-0.0008
Boral sheet on south face . . . . .	-0.122
Boral sheet on west face . . . . .	-0.364
Move to thermal column . . . . .	+0.076

In another test, an aluminum can (6" diameter, 24" long), filled with a solution of water saturated with boric acid was inserted in a beam port adjacent to the reactor. It produced no detectable reactivity change over the previously voided port.

## VI. Void Coefficient of Reactivity

One of the inherent safety features of the swimming-pool type reactor is the negative reactivity coefficient for insertion of voids due to boiling of the moderator. The Borax experiments<sup>(10)</sup> illustrated conclusively that this coefficient is negative. The magnitude of this void coefficient can vary with certain design modifications. For example, the presence of a graphite reflector can affect the void coefficient.<sup>(11)</sup> Part of the initial calibration of the FNR included measurement of this effect.

### Method:

Air was bubbled continuously through one fuel element at a time, varying the flow rate of the air and measuring the effect of the bubbles on the control rod position while maintaining criticality.

The air was passed through a Wet Test (volume) Meter and a manometer. It was then forced down through 8 aluminum tubes (1/32" I.D.) inserted between the fuel plates of the element and bubbled up through the element. The measurements taken were flow rate, air pressure, and position of the control rod. The void volume in the fuel element was then calculated from the barometric pressure, the height of the water above the fuel element and the average velocity of the bubbles.

The bubble velocity was measured by initiating bubbling and measuring the length of time necessary for the bubbles to appear at the top of the fuel element. To keep the bubbles fairly uniform in size and therefore uniform in velocity, they were first passed through a wire screen placed under the fuel plates.

## Results:

This procedure was followed for nine lattice positions, plotting  $\Delta k/k$  against  $\Delta v/v$ , the void ratio for the entire core, where  $v$  is the total water volume in the core. Some representative results are shown in Figure 12. In every case the reactivity dropped sharply as the first 0.08 per cent of void was introduced and then began to decrease at a uniform but lower rate, as the void volume increased to 0.4 per cent.

The values for those lattice positions which were not measured were derived by interpolation. To find an average\* void coefficient, the result for each fuel element was then weighted according to its power output. The data taken and the method of calculation of the void ratio are given in Appendix D.

The fractional void coefficient is defined as the slope of a line drawn from the origin to any point on the averaged curve.  $(\frac{\Delta k}{\Delta v})$  This result is plotted in Figure 13. The steam void coefficient can be calculated by dividing this fractional void coefficient by the volume ( $3.85 \times 10^4$  cc) of the water in the core. Representative void coefficients are presented in Table VIII.

---

\* The effect of variation of void concentration in the vertical direction (during an actual transient) was not included. This would tend to give a higher average void coefficient.

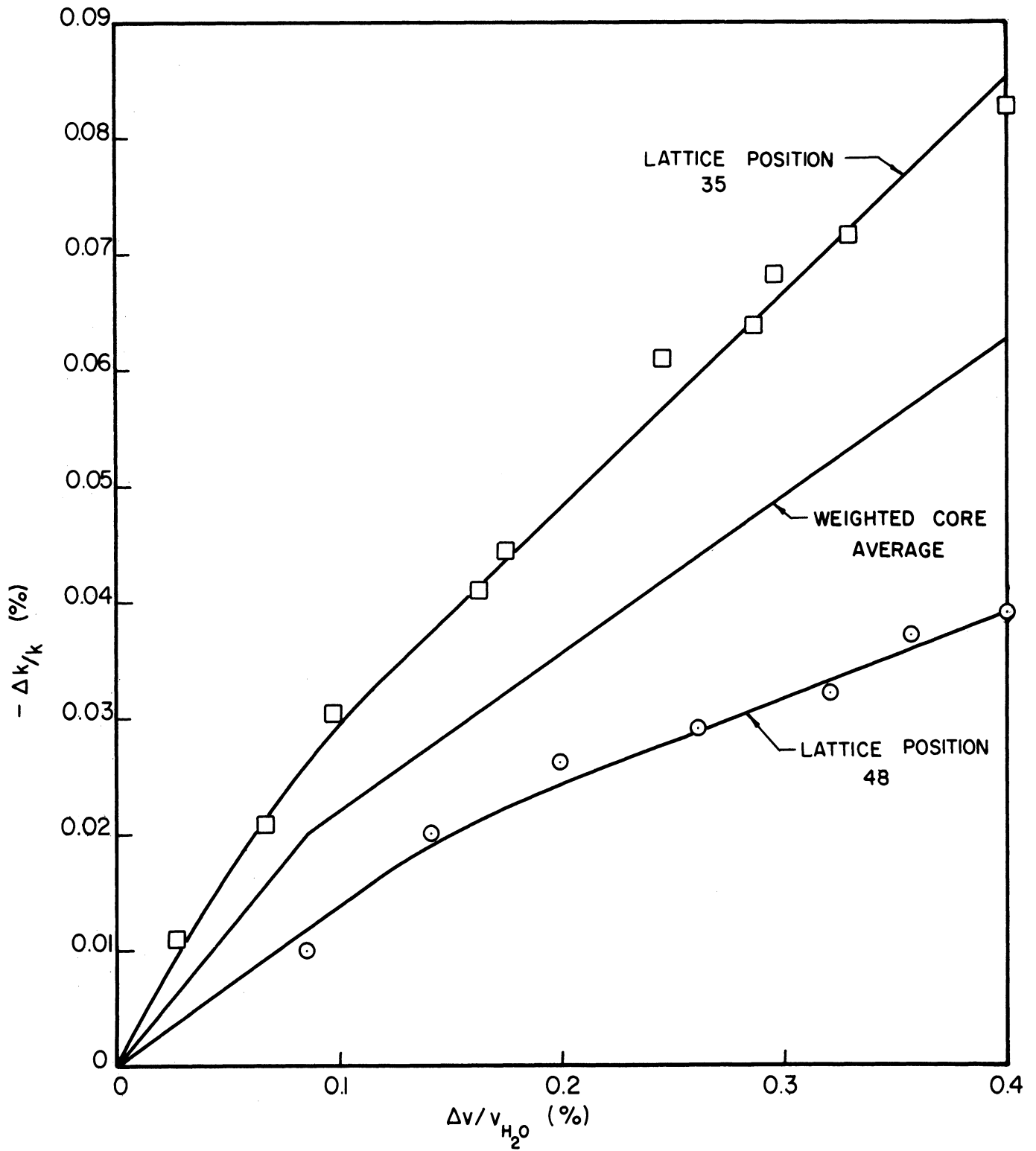


Figure 12.  $-\Delta k/k$  Vs.  $\Delta v/v_{H_2O}$

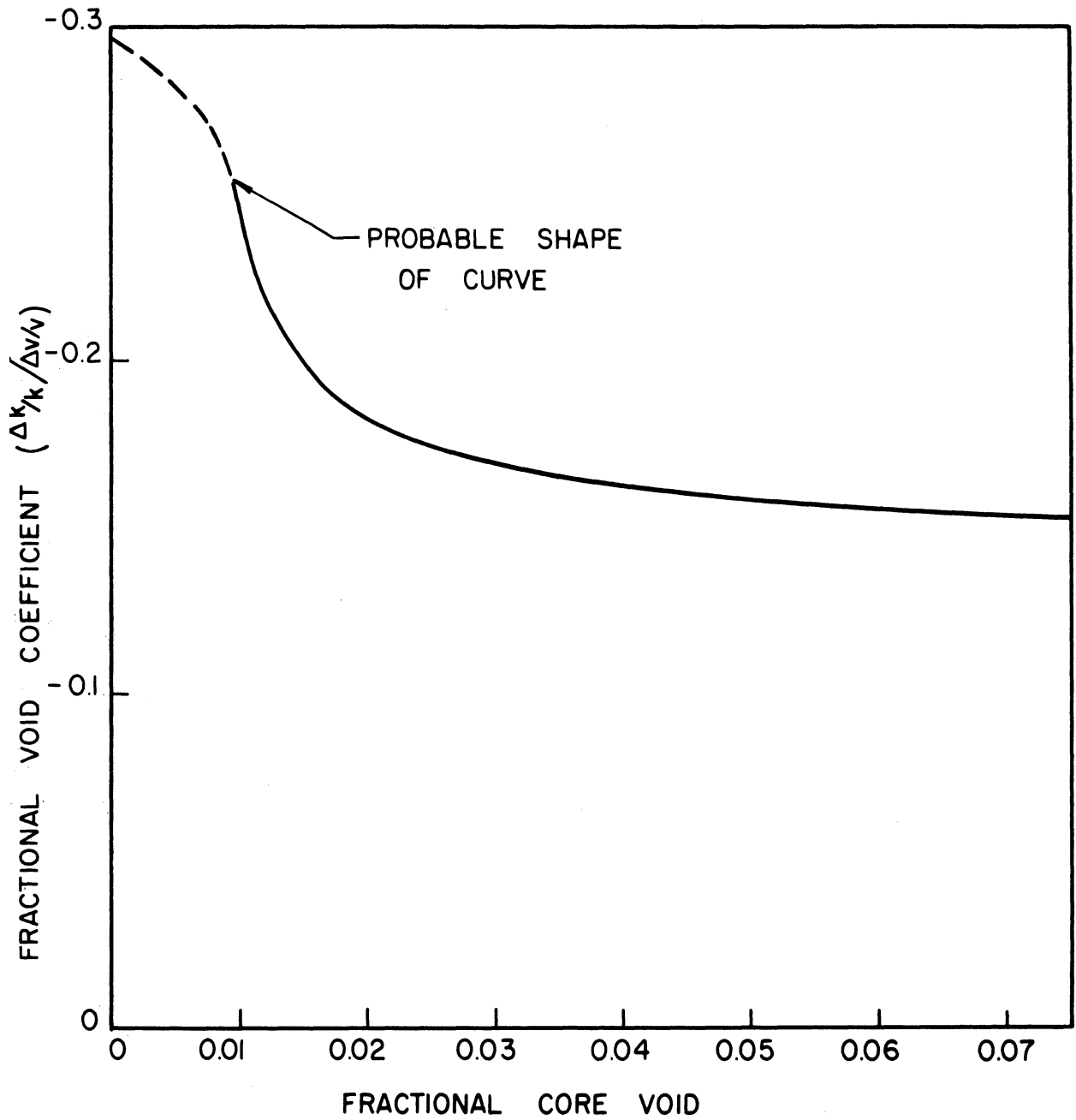


Figure 13. Fractional Void Coefficient Vs. Fractional Core Void. (Void Distributed Uniformly in the Vertical Direction and Proportional to Power in the Horizontal Direction.)

TABLE VIII

## Representative Void Coefficients

<u>Amount of Core Voided</u>	<u>Fractional Void Coefficient</u>	<u>Steam (<math>\Delta k/k</math> per cc) Void Coefficient</u>
1 per cent	-0.247	$-6.41 \times 10^{-6}$
6 per cent	-0.156	$-4.05 \times 10^{-6}$

---

It is probable that during an actual power excursion the observed void coefficient would be greater than these values by at least 10 per cent, due to the concentration of the void at the center of the core.

The estimated error in these values of void coefficients is  $\pm 15$  per cent. This error results largely from discrepancies in the measurements of bubble velocities.





## VII. RADIATION SURVEY

A radiation survey of the reactor building was made with the reactor operating at 100 kilowatts. All of the beam ports were plugged and flooded. The primary coolant flow was turned off. The pool water level was even with the overflow trough and the reactor core was located at the beam port position at the north end of the pool.

Except for that area of the basement immediately beneath the reactor, no occupiable space within the Reactor Building was found to have a radiation level exceeding 1.6 milliroentgens per hour (mr/hr.). This level occurred at the pool surface directly above the core. All of the other areas in the building had levels below 0.2 mr/hr. No neutrons (fast or slow) were detected at any location in the building.

Gamma radiation levels below 2 mr/hr were measured with a Nuclear Instrument Company Geiger-Mueller survey instrument. Higher gamma levels were measured with a Technical Associates (Juno) ionization chamber survey meter. Both instruments were calibrated on the day of the survey with a 361 millicurie cobalt-60 source. Neutrons were measured with a Radiation Counter Lab portable neutron survey meter. Gamma radiation levels reported in the following table are above background.

TABLE VIII

## GAMMA RADIATION LEVELS AT 100 KW

<u>General Location</u>	<u>mr/hr</u>	<u>Specific Location of Detectable Readings</u>
Third Floor	0.2	Water surface at middle of pool
	0.15	Center of reactor bridge
	0.2	Chest height at north end of pool
	1.6	Water surface above reactor core
Second Floor	0.0	No detectable readings above background
First Floor	0.02	4 inch access ports on north face of tank
	0.02	All 14 port faces
Basement	0.0	Entrance door
	0.02	Under hatch cover
	0.15	Front of heat exchanger
	1.3	At primary pump
	0.0	In front of hot demineralizer tank
	5.5	East end of hold up tank
	1.2	Entrance to passageway to area beneath reactor
	8.5	Middle of passageway
	150.	Entrance to area beneath reactor
	2500.	Chest height beneath reactor core
4700.	On ceiling beneath core	
5000.	Pneumatic tube bundle entrance to pool	

## VIII. POWER CHECK AT 100 KW

With the increase in reactor power to 100 kw, the Log N chamber was raised away from the core so as to decrease the strength of the signal to the instrument by a factor of 40. Based on previous data from low power level work, when the Log N channel indicates 100, the reactor should be operating at a power level of 110 kw  $\pm$  9.9 kw. (The initial power was calculated as 0.58 watts with a Log N reading of 0.021. Then 0.58 watts multiplied by  $1.9 \times 10^5$  yields 110 kw.)

After this change in the position of the Log N chamber was made, two methods were used to recalibrate the power indication. In the first, a gold foil was irradiated at a precisely located position in the core for a fixed length of time. The induced radioactivity was then measured and compared with the activity which had been induced in a similar foil used during the initial low power calibration studies.

The second method involved measurements of the gamma dose rates at known distances from the side of the core and comparing them with the dose rates obtained at the Bulk Shielding Facility for a similar lattice configuration. The gamma dose rates were measured using the ferrous-ferric dosimetry technique.

The results of the latter method are shown in Figure 14 and indicate that the reactor was operating at approximately 115 kw at the time the measurement was made. The results of the gold foil irradiation indicate that the reactor was operating at a power level of 101 kw  $\pm$  9.1 kw (assuming same errors as in original measurement). These results, at a nominal power level of 100 kw, indicated that the reactor was close to the desired power and no further adjustments were made.

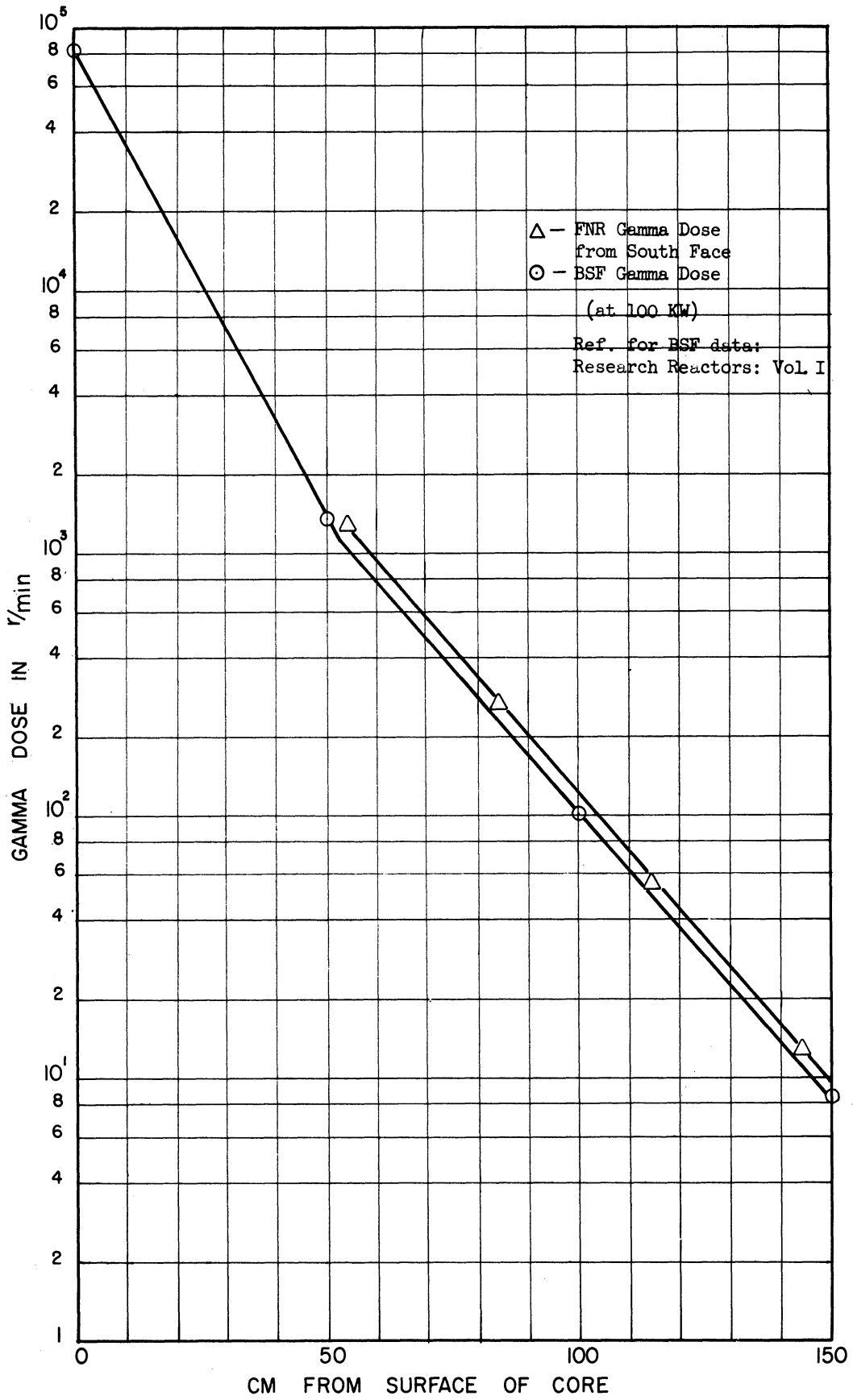


Figure 14

Approximately three months after the reactor was first operated at 100 kw, and after many hours of operation at 100 kw, the power level was again measured. The same methods for power measurement were used (with the exception that four gold foils, instead of one, were irradiated) and the results compared. The gold foil activities indicated that the power level was  $107 \pm 9.6$  kw and that the gamma dose rate measurement indicated a power level of approximately 120 kw.

A calorimetric check of the power level is planned to provide a third method of measurement at higher powers (100 kw to 1000 kw).

## IX. TEMPERATURES AT 100 KW

The temperature of the water between the fuel plates was measured while the reactor was operating at 100 kw. A copper-constantan thermocouple attached to a probe was lowered into successive fuel elements. The temperatures were read on a standard millivolt recorder to an accuracy of  $\pm 0.5^{\circ}\text{F}$ .

TABLE IX  
Water Temperature at 100 Kw

Exp. #	Lattice Position	TEMPERATURES ( $^{\circ}\text{F}$ )				
		1	2	3	4	5
66 (1-30-58)	48	72*	--	89*	96*	98*
	35	78	84	91	98	101
	27	77	78	85	93	97
67 (1-31-58)	55	75	80	88	95	99
	45	73	82	90	97	100
	54	77	82	90	96	99
	57	77	80	88	95	99
	56	78	84	92	98	101
69 (2-4-58)	33	77	80	88	94	96
	34	77	81	89	97	100
	36	79	83	90	98	102
	37	77	82	89	96	100
	25	78	82	88	96	100

\*Thermocouple was placed 2" too low for these readings.

Temperature (1) 12" below core midplane

(2) 6" " " "

(3) midplane

(4) 6" Above midplane

(5) 12" " "

## X. CONCLUSION

On the basis of the work reported herein, it is the conclusion of the calibration personnel that the stability and safety of reactor operation at power levels up to 100 kw has been demonstrated. There are, of course, many other useful and interesting measurements which can and will be made. For example, the neutron flux and spectra in the beam ports will be measured as well as the flux distribution in the thermal column. Also a reactor oscillator is presently being designed to measure the reactor transfer function. These and other experiments are planned in conjunction with the nuclear engineering laboratory course.

Although much valuable work can be done at 100 kw or less, there are many applications for which higher powers are required. Experiments in neutron diffraction, activation analysis, and metallurgical effects of radiation are presently being designed. For these, a power level of 1 Mw is essential. Even more important at this time is the need to check the reactor and cooling system performance under full load (1 Mw) so that any faults may be promptly corrected. It is our conclusion that tests at 1 Megawatt should proceed without delay.





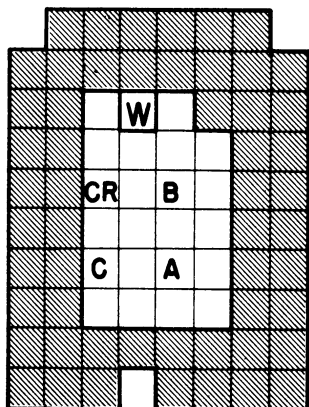
## REFERENCES

1. Abernathy, Fred H., et al. A low cost experimental neutron chain reactor. Part 2. U.S. Atomic Energy Commission, report CF 52-11-125. August 20, 1952.
2. Riseng, O. A. J., Stone, Philip M. and Vélez, Carlos. Two group, three region solutions of the flux and adjoint junction for a finite cylindrical approximation to the Ford Nuclear Reactor, and their use in perturbation theory. M.S. Thesis, University of Michigan, July 1956.
3. Meem, J. L. and Johnson, E. B. Determination of the power of the shield-testing reactor. Part 1. Neutron flux measurements in the water-reflected reactor. U.S. Atomic Energy Commission, report ORNL 1027. August 13, 1951.
4. Martin, David H. Correction factors for measurements with cadmium covered foils. U.S. Atomic Energy Commission, report NAA-SR 1076. October 15, 1954.
5. Meem, J. L., Holland, L. B. and McCammon, G. M. Determination of the power of the Bulk Shielding Reactor. Part 3. Measurement of the energy released per fission. U.S. Atomic Energy Commission, report ORNL 1537. March 11, 1954.
6. Meem, J. L., Johnson, E. B. and Hungerford, H. E. Energy per fission and power of the Bulk Shielding Reactor. U.S. Atomic Energy Commission, report AECD 3931. May 12, 1953.
7. Cochran, R. G., et al. Reactivity measurements with the Bulk Shielding Reactor. U.S. Atomic Energy Commission, report ORNL 1682. November 19, 1954.
8. Moore, R. A., Nance, J. C. and Perry, L. W. GTR rod calibration. Convair, ANP document number NARF 54-14T. March 30, 1955.
9. Hogerton, J. F. and Grass, R. C., eds. The reactor handbook. Volume 1. Physics. U.S. Atomic Energy Commission, report AECD 3645. June 1953. P. 539
10. Ulrich, A. J. Results of recent analyses of Borax II transient experiments. U.S. Atomic Energy Commission, report ANL 5532. April 1956.
11. Pigford, Thomas H., et al. Neutron lifetimes and void coefficients for research reactors. Cleveland, Nuclear Engineering and Science Congress, preprint 154. December 1955.
12. Luckow, William K. and Widdoes, Lawrence C. Cost data on the University of Michigan Research Reactor. Nucleonics 13, no. 6: 104-6, June 1955
13. Ricker, Charles W. and Gomberg, Henry J. Control system of the Ford Nuclear Reactor. ISA Journal 4: 496-501, November 1957.
14. Michigan. University. Michigan Memorial-Phoenix Project. The Ford Nuclear Reactor: Description and operation. June 1957.
15. Federal Register 22: 6998-7000, August 30, 1957.
16. Meinke, W. W., Emmons, A. H. and Gomberg, H. J. A versatile hot lab for university research. Nucleonics 13, no. 11: 76-79, November 1955.



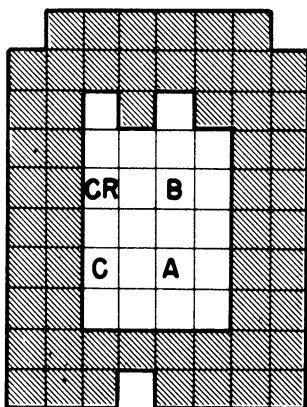
APPENDIX A

The following configurations have been brought to criticality.  
No data other than the critical mass is available:

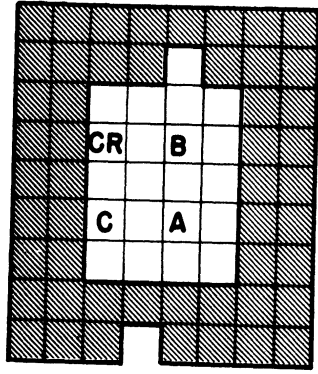


Loaded mass = 2680 gm.  
Critical mass = 2633 gm.

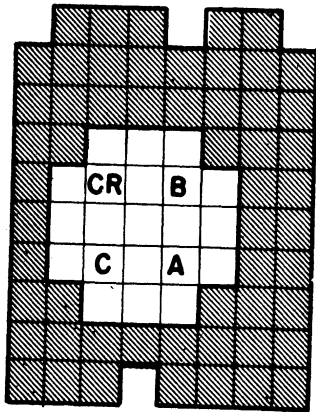
W = no element in this position  
(water hole).



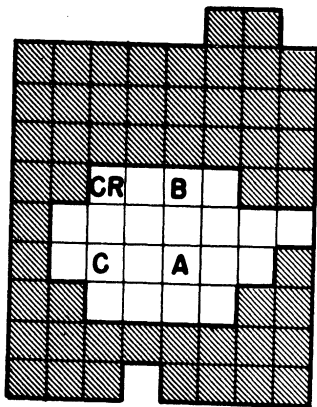
Loaded mass = 2680 gm.  
Critical mass = 2554 gm.



Loaded mass = 2539 gm.  
 Critical mass = 2513 gm.



Loaded mass = 2538 gm.  
 Critical mass = 2470 gm.



Loaded mass = 2538 gm.  
 Critical mass = 2526 gm.

## APPENDIX B

This section contains a tabulation of bare foil saturated activities (Table B-I). Figures B-1, B-2, and B-3 show the variation of cadmium ratio throughout the core. These curves were plotted from the curves of cadmium ratio for each fuel element, shown in Figures B-4 and B-5.

Figures B-6 and B-7 are curves plotted from the data in Table B-I. The variation of thermal flux in each fuel element is shown in Figures B-8, B-9, and B-10.

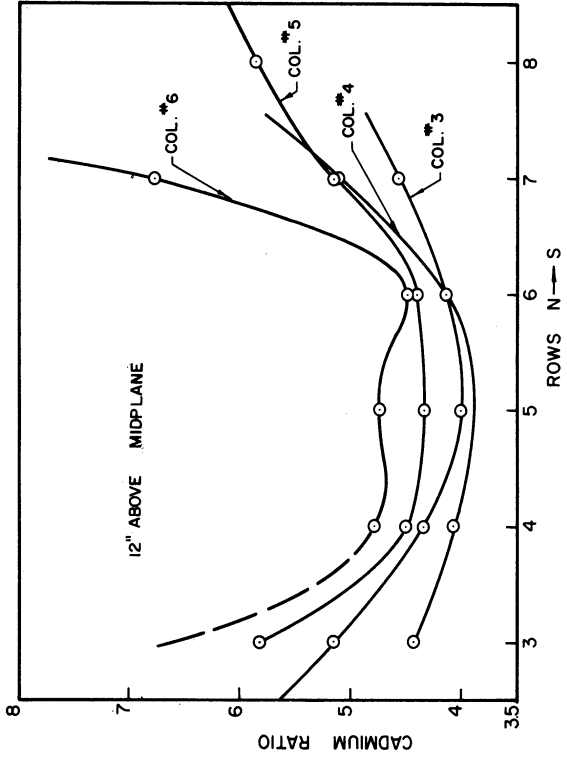


Figure B-1

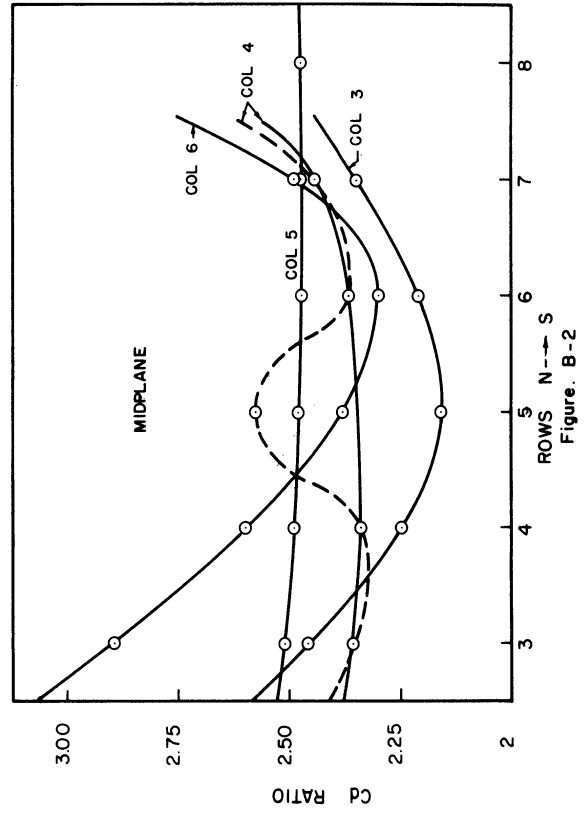


Figure B-2

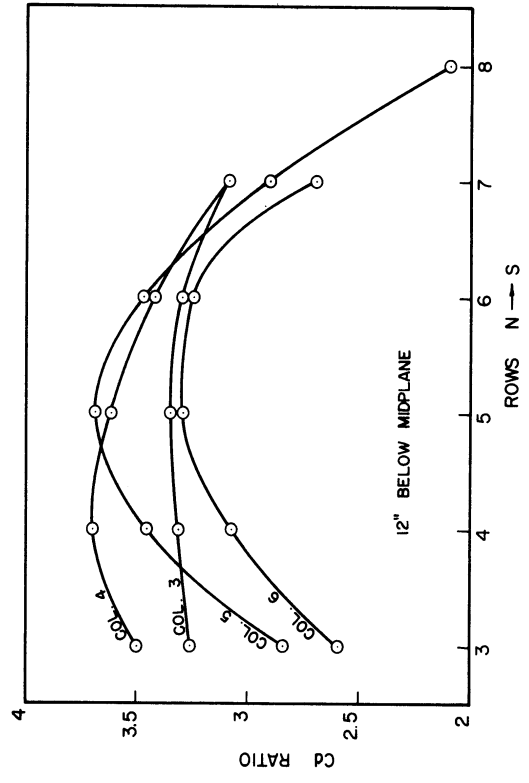


Figure B-3

AVERAGED VALUES OF CADMIUM RATIO

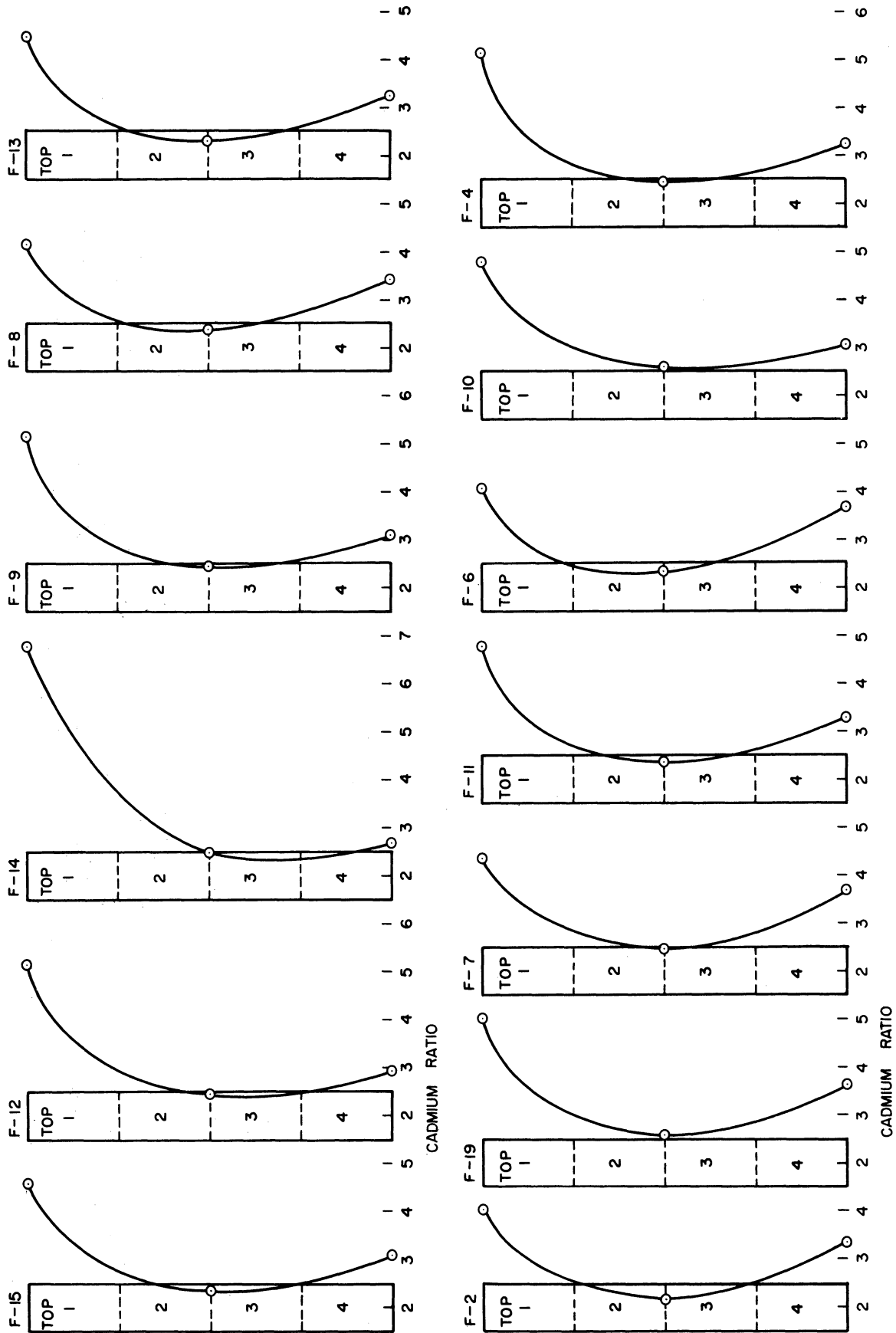
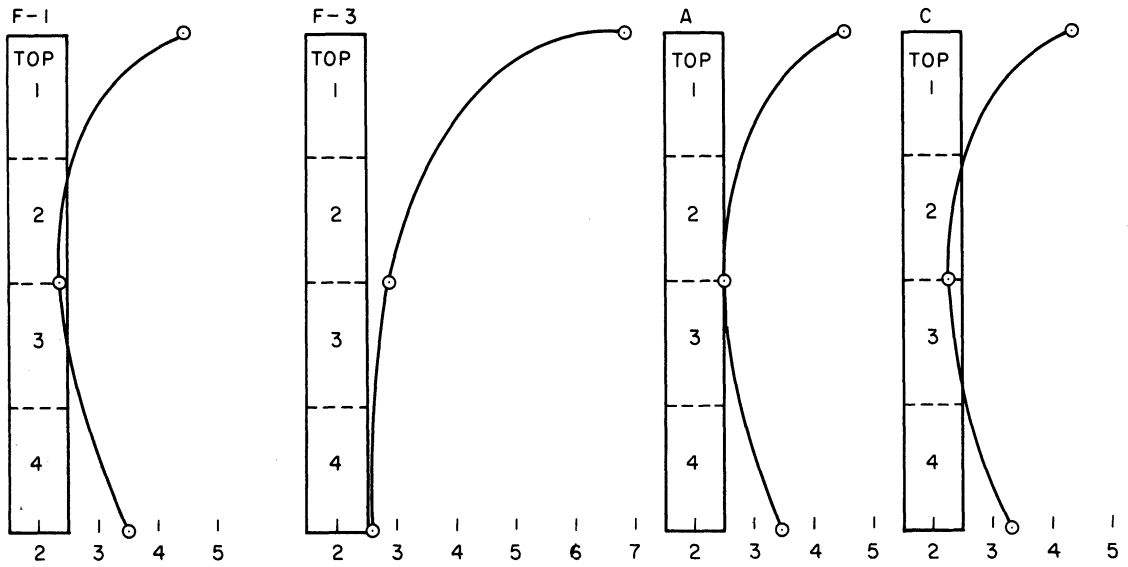
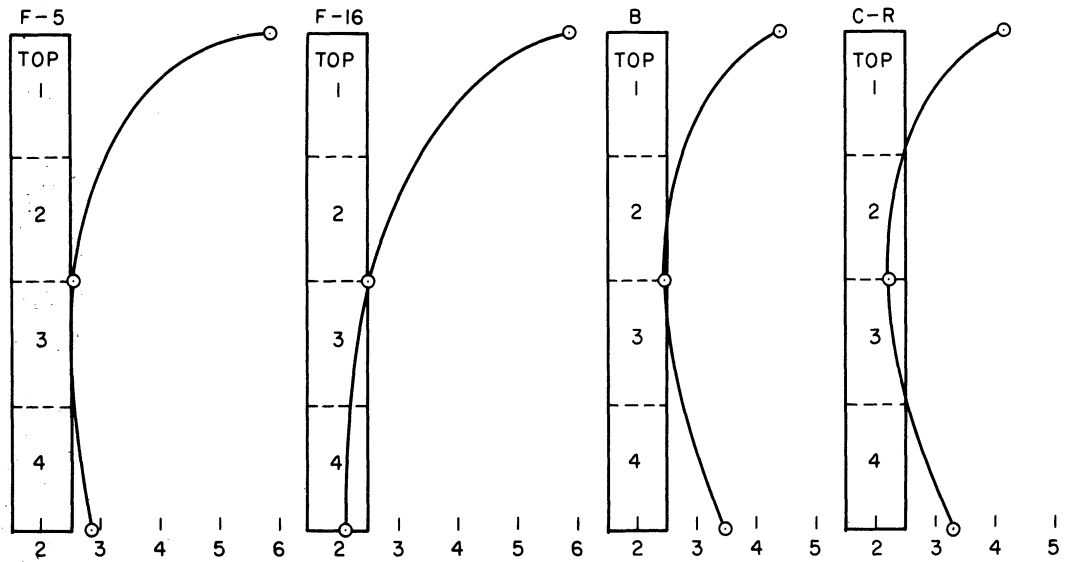


FIGURE B-4 CADMIUM RATIOS FROM TOP TO BOTTOM OF FUEL ELEMENTS  
(SEE FIG. B7 FOR LATTICE POSITION OF FUEL ELEMENTS)



CADMIUM RATIO



CADMIUM RATIO

FIGURE B-5 CADMIUM RATIOS FROM TOP TO BOTTOM OF FUEL ELEMENTS.  
 (SEE FIG. B7 FOR LATTICE POSITION OF FUEL ELEMENTS)



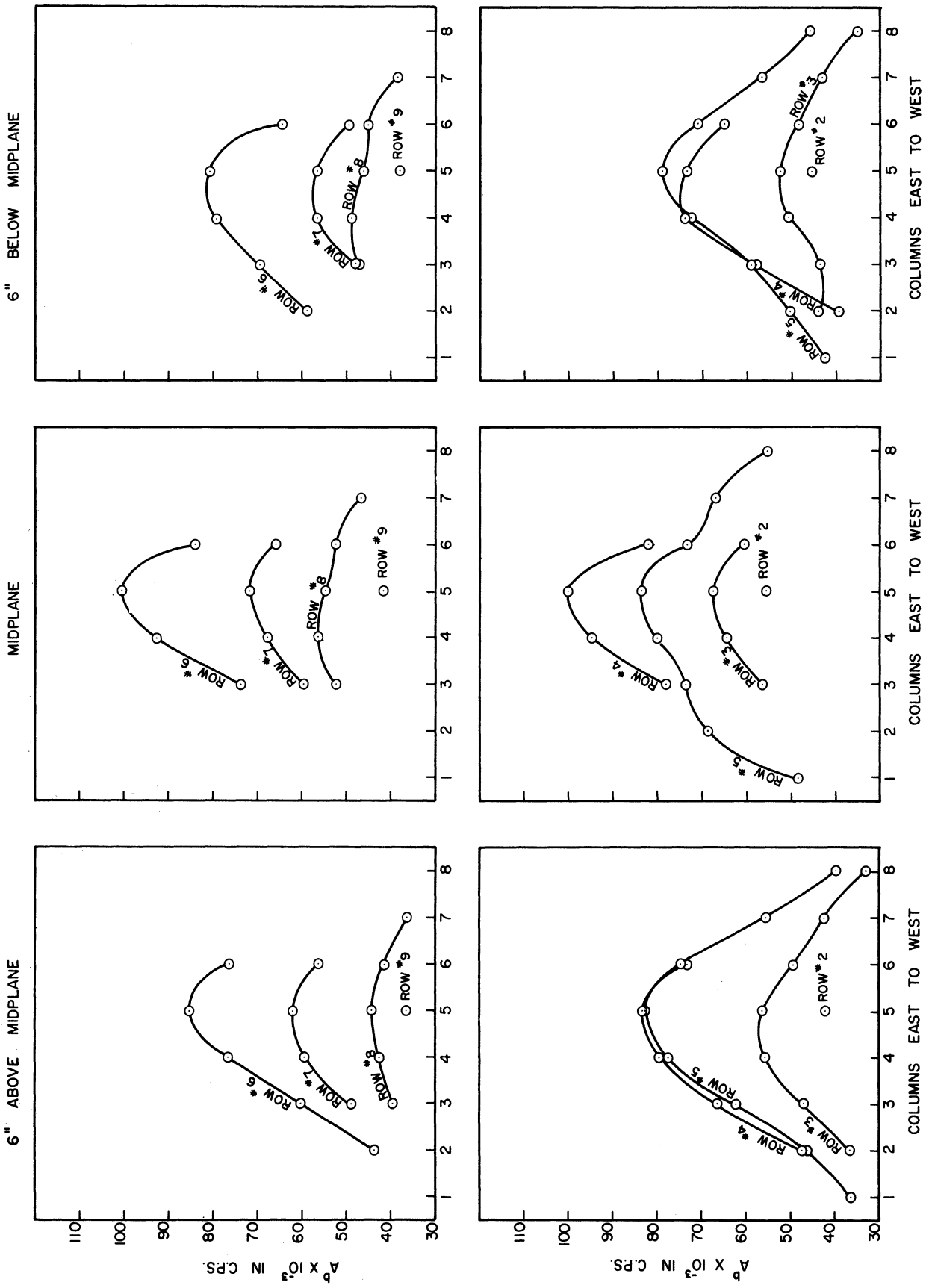


FIGURE B-6 SATURATED GOLD FOIL ACTIVITIES.



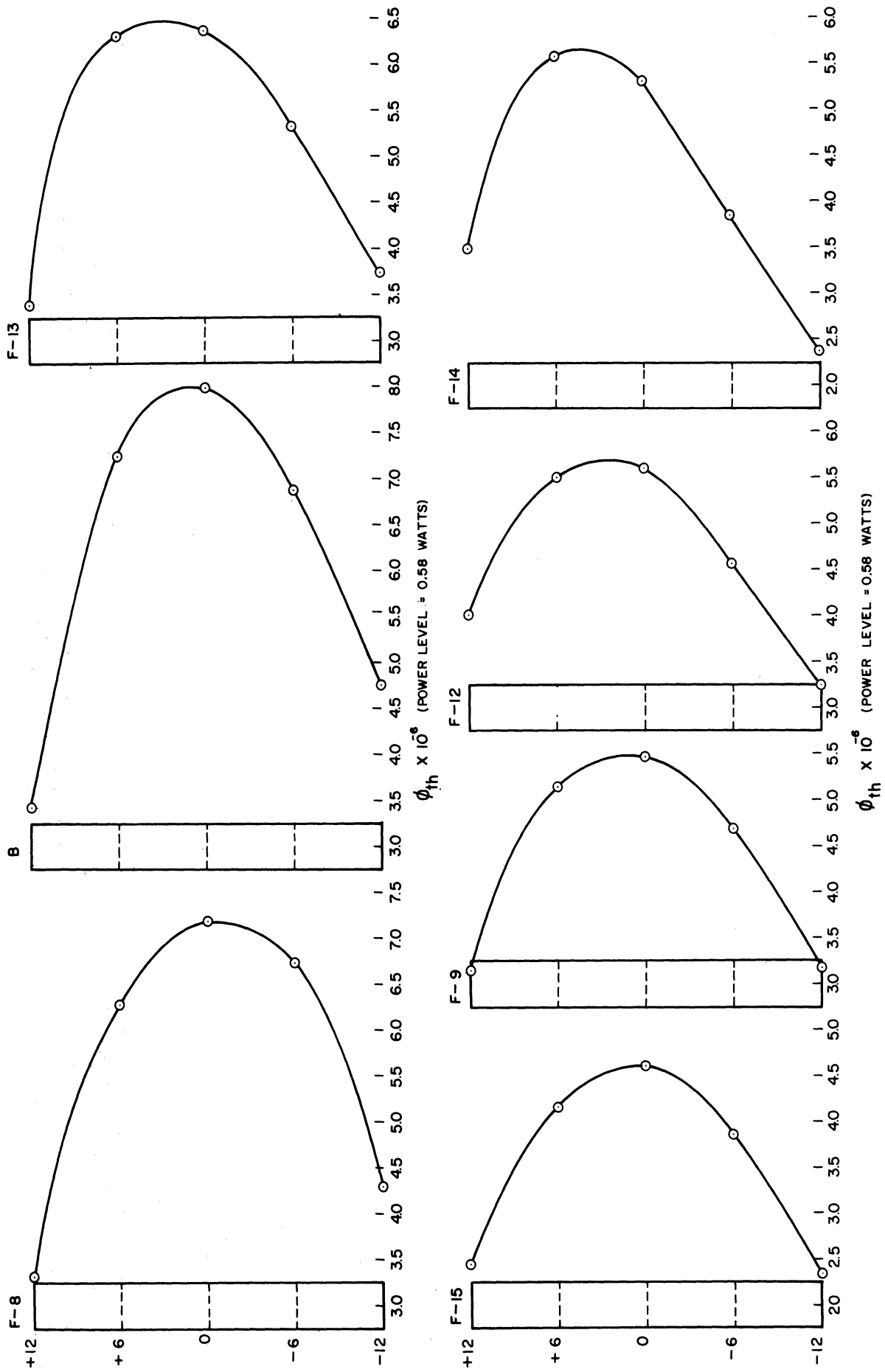


FIGURE B-8 THERMAL FLUX FROM TOP TO BOTTOM OF FUEL ELEMENTS  
(SEE FIG. B-7 FOR LATTICE POSITION OF FUEL ELEMENTS.)

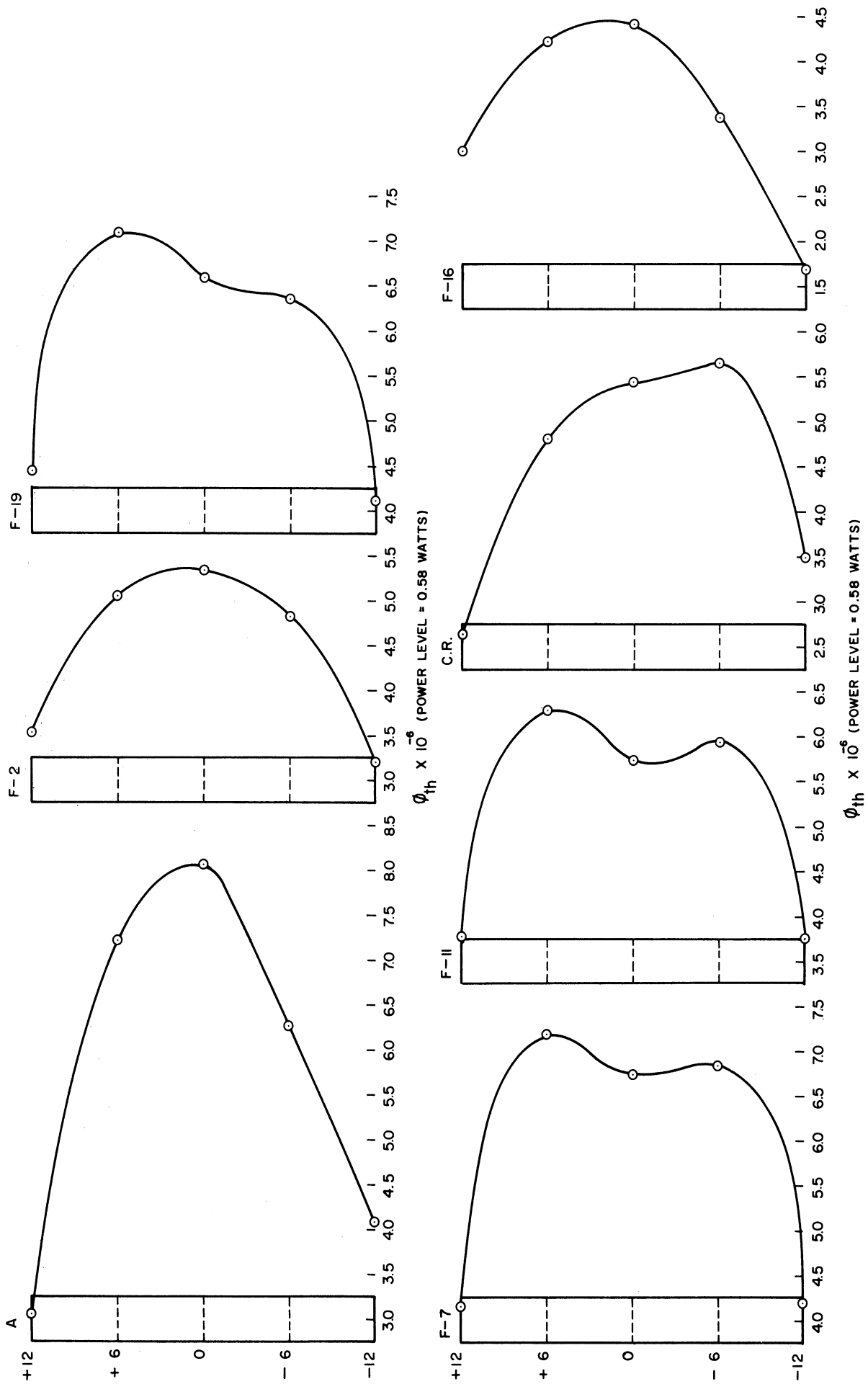


FIGURE B-9 THERMAL FLUX FROM TOP TO BOTTOM OF FUEL ELEMENTS.  
(SEE FIG. B-7 FOR LATTICE POSITION OF FUEL ELEMENTS)

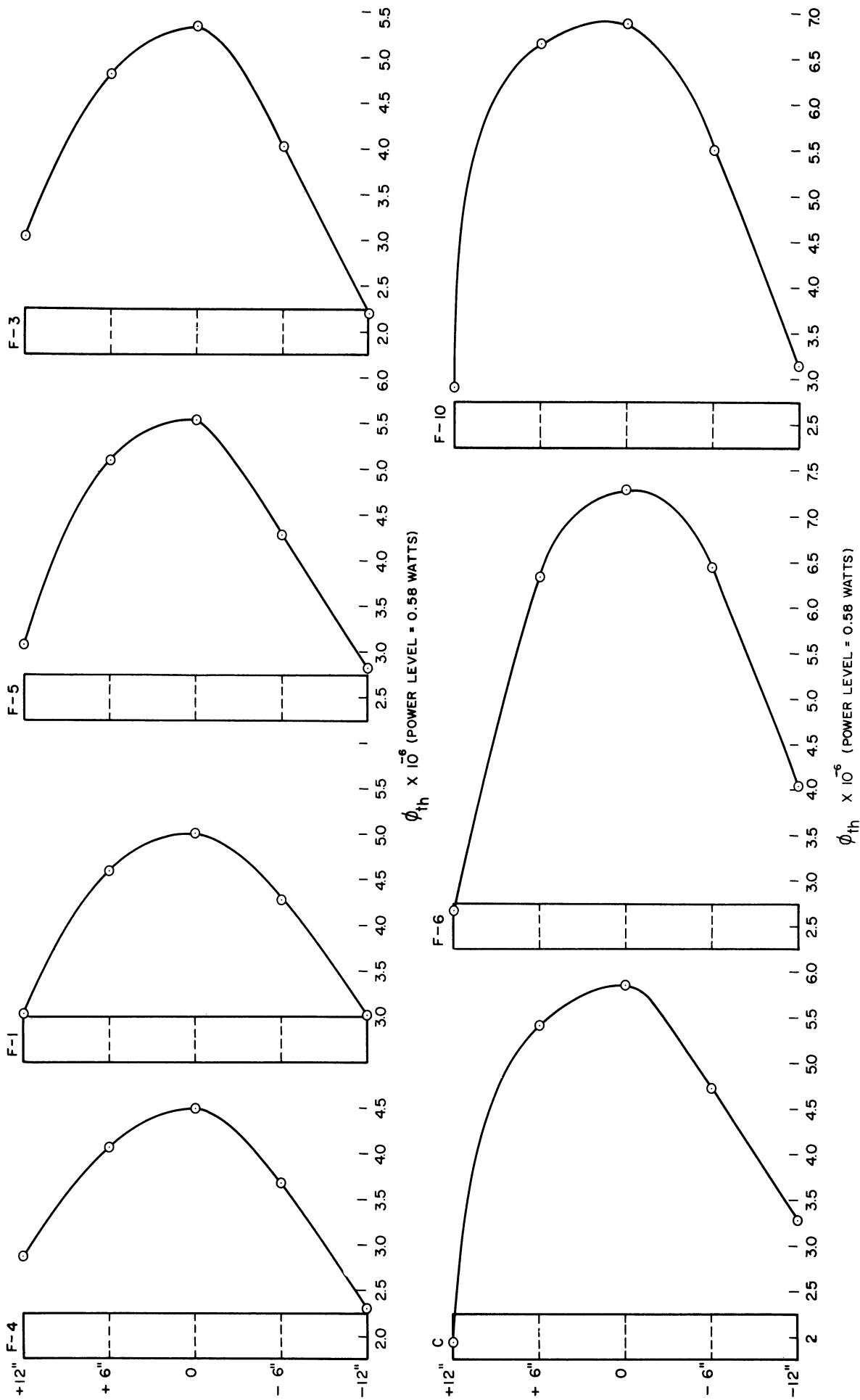


FIGURE B-10 THERMAL FLUX FROM TOP TO BOTTOM OF FUEL ELEMENTS.  
(SEE FIG. B-7 FOR LATTICE POSITION OF FUEL ELEMENTS)

TABLE B-I

Bare Foil Saturated Activities

<u>Position</u>	<u><math>A_s^b \times 10^{-4}</math></u>	<u>Position</u>	<u><math>A_s^b \times 10^{-4}</math></u>	<u>Position</u>	<u><math>A_s^b \times 10^{-4}</math></u>
23 E 1	3.30	24 E 1	2.26	25 E 1	4.39
2	5.97	2	8.04	2	7.55
3	7.57	3	10.16	3	11.50
4	5.41	4	6.13	4	7.24
5	2.97	5	4.38	5	3.96
23 W 1	4.29	24 W 1	3.10	25 W 1	5.60
2	7.51	2	11.00	2	10.27
3	8.59	3	12.23	3	9.61
4	7.09	4	10.47	4	9.75
5	4.11	5	5.61	5	5.75
33 W 1	4.04	34 W 1	4.42	35 W 1	6.23
2	8.47	2	11.72	2	12.00
3	9.93	3	14.82	3	13.33
4	7.33	4	10.83	4	11.00
5	4.90	5	6.23	5	6.33
43 W 1	3.85	44 W 1	3.94	45 W 1	5.26
2	7.60	2	12.15	2	11.71
3	9.42	3	13.80	3	10.67
4	7.71	4	10.23	4	11.62
5	4.36	5	6.00	5	6.77
53 W 1	3.76	54 W 1	3.89	55 W 1	4.88
2	6.58	2	8.81	2	9.67
3	7.99	3	9.71	3	10.36
4	6.19	4	8.37	4	8.76
5	3.32	5	3.92	5	4.71

TABLE B-I (Continued)

Bare Foil Saturated Activities

<u>Position</u>	<u><math>A_s^b \times 10^{-4}</math></u>	<u>Position</u>	<u><math>A_s^b \times 10^{-4}</math></u>	<u>Position</u>	<u><math>A_s^b \times 10^{-4}</math></u>
26 E 1	2.98	27 E 1	3.75	28 E 1	3.87
2	6.96	2	6.50	2	6.40
3	9.67	3	7.79	3	7.97
4	9.71	4	6.14	4	6.57
5	5.02	5	3.04	5	3.50
26 W 1	4.37	27 W 1	2.92	28 W 1	3.83
2	10.23	2	7.47	2	6.35
3	11.43	3	9.29	3	7.72
4	10.27	4	7.58	4	6.69
5	5.65	5	4.37	5	3.41
36 W 1	4.95	37 W 1	5.40	56 W 1	4.77
2	11.65	2	9.47	2	91.35
3	15.00	3	10.27	3	10.29
4	12.41	4	8.63	4	7.71
5	7.26	5	5.70	5	4.58
46 W 1	4.51	47 W 1	5.20	57 W 1	3.52
2	12.71	2	8.25	2	7.84
3	13.73	3	10.27	3	8.62
4	10.69	4	7.62	4	6.55
5	6.89	5	4.79	5	3.27





## APPENDIX C

### SAMPLE POWER CALCULATION

The following calculations illustrate the procedure used to calculate the reactor power from activated gold foil data.

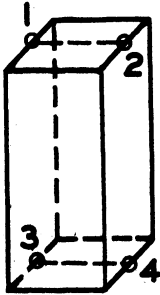


Figure C-1

Placement of foils to define a power cell equal to one quarter of a fuel element.

	$A_s^b$ *	Horizontal Average
Foil 1	96115	
Foil 2	133270	114693
Foil 3	97508	
Foil 4	110045	103777

This averaging process gives two numbers which are proportional to the total flux at the top and at the bottom of the power cell. The saturated thermal activity is then found by multiplying these averages by the factor  $(1 - \frac{1}{CR})$ , which is found as follows:

$$A_s^{th} = A_s^b - \frac{A_s^b}{CR} = A_s^b \left(1 - \frac{1}{CR}\right), \text{ where } CR = \text{cadmium ratio.}$$

\* Values for third cell of fuel element number 19, lattice position 35.

For this particular power cell the cadmium ratios and the corresponding factors are:

	<u>CR</u>	$\frac{(1 - 1)}{\text{CR}}$
Top	2.58	.612
Bottom	2.87	.651

Using these cadmium ratio values and the average saturated bare activities, the following values of saturated thermal activity are computed.

	$\frac{A_{th}}{A_s^{th}}$
Top	70192
Bottom	67559

At this point the average saturated thermal activity of this power cell could be found, but to facilitate the plotting of  $\phi_{th}$ , the vertical averaging was not done until  $\phi_{th}$  had been calculated for the top and bottom of each cell.

From the standard gold foils irradiated at Argonne National Laboratory, it is concluded that:

$$\frac{\phi_{th}^{ANL}}{A_{th}^s (ANL)} = 93.94 \text{ (avg. of two foils)}$$

Multiplying the saturated thermal activities from the Ford Reactor by this factor will give  $\phi_{th}$ .

	$\phi_{th}$	Average for Power Cell
Top	$6.59 \times 10^6$	} $6.47 \times 10^6 \text{ n/cm}^2 \text{ sec}$
Bottom	$6.35 \times 10^6$	

This value of  $\phi_{th}$  is used in the following equation to find the power of one cell:

$$P = \frac{(\sigma_f)(E)(G)(\phi)(6.02 \times 10^{23})}{A}$$

where:

E = energy per fission = 193 mev

G = grams of fuel in this particular power cell

$\phi$  = average thermal flux in this cell

A = atomic weight of U = 235

$\sigma_f$  = fission cross section = 580 barns.

Then the power for this particular cell is:

$$P = \frac{(193)(1.6 \times 10^{-13})(35.25)(6.47 \times 10^6)(6.02 \times 10^{23})(580 \times 10^{-24})}{235}$$

P = 0.0105 watts.



## APPENDIX D

### CALCULATION OF VOID RATIO

The void ratio is defined as the ratio of bubble volume to total moderator volume before bubbling. The three major assumptions made in measuring the void ratio were:

1. The mass flow rate of air through the fuel element was equal to the mass flow rate of air through the Wet Test Meter.
2. The average velocity of the bubbles through the fuel element was constant throughout the experiment.
3. The void distribution was uniform throughout the fuel element.

The velocity of the bubbles was measured as  $1.10 \pm 0.05$  feet per second. This measurement, made by starting bubble flow and measuring the time for the first bubble to appear at the top of the element, was rather crude. It did not necessarily represent an average velocity for a particular bubble size distribution. The void coefficient is inversely proportional to the average velocity and, therefore, the shape of the curve, which is the most interesting result of the experiment, was not affected by errors in this measurement.

Following assumption 3, the area ratio will be the same as the void ratio.

Thus:

$$\text{Void Ratio} = \frac{Q_1 P_1}{P_2 V_2 A_{H_2O}}$$

where:

$Q_1$  = air flow rate through the Wet Test Meter

$P_1$  = pressure at meter (absolute)

$P_2$  = pressure at midpoint of fuel element (absolute)

$V_2$  = average bubble velocity

$A_{H_2O}$  = total moderator cross sectional area in core.

The source of air for the experiment was the 60 psi laboratory compressed air. It was found that fluctuations in the input pressure to the fuel element could not be eliminated even with a pressure regulating valve. Therefore, many runs were made holding the pressure as constant as possible while at the same time the flow rate was measured with the Wet Test Meter and a stop watch. The flow rate was then plotted (see Figure D-1) as a function of the difference between the applied pressure and the water pressure at the midpoint of the fuel element. This curve was used in the actual experiments and the meter was removed. To see if removing the meter had any effect on the flow rate, a curve of void ratio versus reactivity was plotted with and without the meter for a fuel element position. This showed a deviation indicating an increase in flow of 10%. All the void ratios were increased by this factor of 10%.

Sample Calculation:

Exp. #61. Barometer: 74.6 cm Hg.

Water height: 21' 2"

Run #6. Gauge air pressure = 83.9 cm Hg.

Total water pressure = 74.6 + 47.5 = 122.1 cm.

Total air pressure = 74.6 + 83.9 = 158.5 cm.

Pressure difference = 36.4 cm.

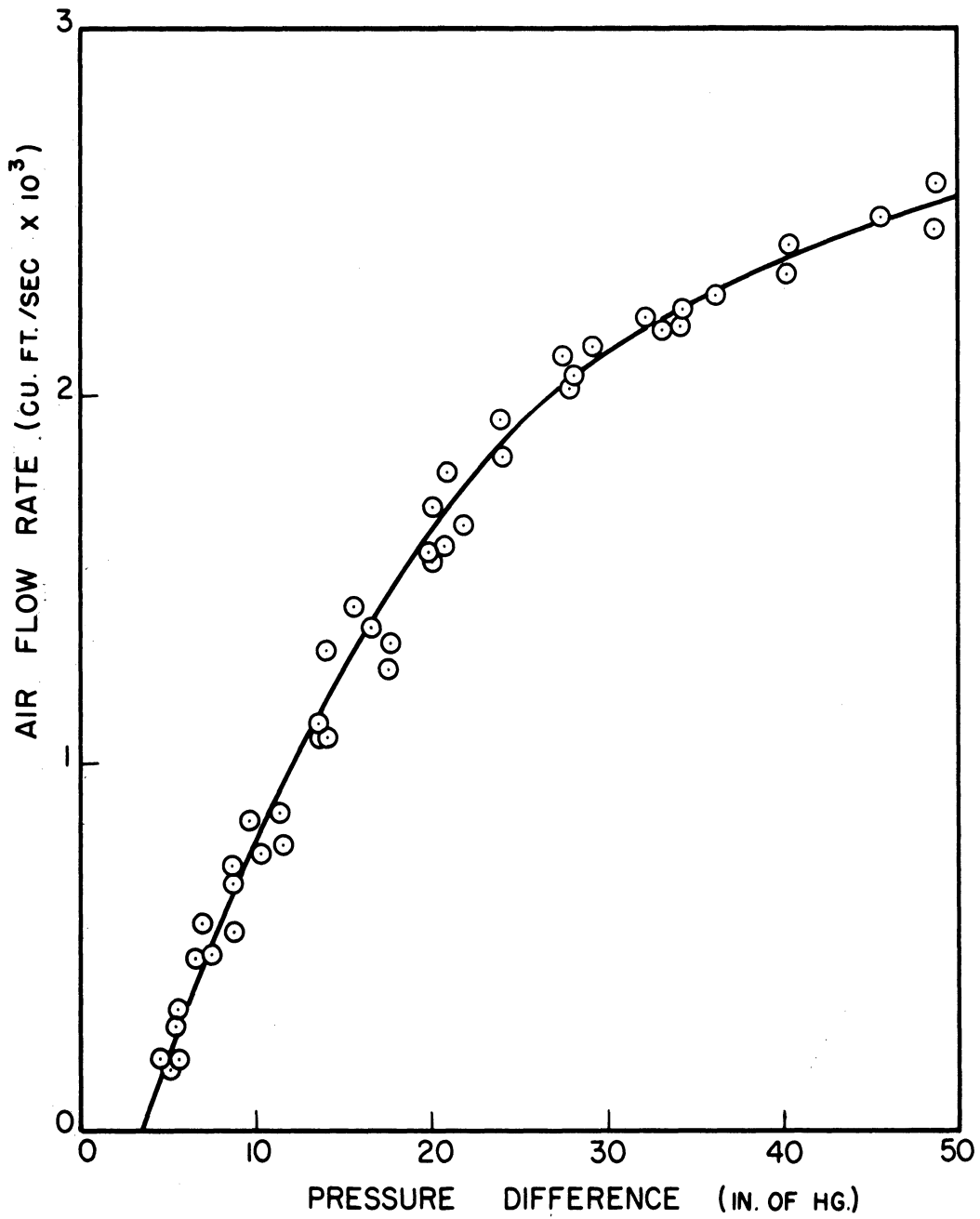


Figure D-1. Air Flow Rate Vs. Pressure Difference (as Measured With the Wet Test Meter).

Flow rate (from Figure D-1) =  $0.00229 \text{ ft}^3/\text{sec}$

$$\text{Void Ratio} = \frac{1.1(0.00229) \times 158.5}{122.1 \times 1.1 \times 0.84} = 0.003540$$

The cross-sectional water area per fuel element is  $0.04 \text{ ft}^2$ .

Therefore, the total cross sectional water area is  $0.84 \text{ ft}^2$ .

The factor 1.1 in the numerator of the above expression is the 10% correction to flow rate mentioned above. The factor 1.1 in the denominator is the bubble velocity in feet per second.



TABLE D-I

Void Coefficient Data

Exp. #61, Barometer: 74.6 cm. Hg., Water Height: 21' 2"

<u>Lattice Position</u>	<u>Run #</u>	<u>Gauge Air Pressure (Cm. Hg.)</u>	<u>Control Rod (In.)</u>	<u><math>\Delta k/k(\%)</math></u>	<u>Flow Rate <math>\times 10^3</math> (ft<sup>3</sup>/sec)</u>	<u><math>\Delta v/v(\%)</math></u>
27	1	0.0	25 9/16	0.0	0.0	0.0
	2	55.9	24 5/16	0.0125	0.630	0.0802
	3	60.0	24 3/4	0.0160	1.05	0.1379
	4	70.4	24 11/32	0.0255	1.82	0.2565
	5	75.5	24 1/16	0.0300	2.05	0.3005
	6	83.9	23 11/16	0.0380	2.29	0.3540
	7	91.4	23 5/8	0.0385	2.44	0.3950
	8	64.2	24 19/32	0.0200	1.40	0.1895
	9	83.0	23 3/4	0.0360	2.27	0.3480
34	1	0.0	25 1/2	0.0	0.0	0.0
	2	55.9	24 19/32	0.018	0.630	0.0802
	3	60.0	24	0.030	1.05	0.1379
	4	64.2	23 1/2	0.040	1.40	0.1895
	5	70.4	23 3/32	0.047	1.82	0.2565
	6	75.5	22 7/8	0.051	2.05	0.3005
	7	83.9	22 17/32	0.058	2.29	0.3540
	8	91.4	22 1/4	0.064	2.44	0.3950

Exp. #62, Barometer: 75.9 cm. Hg., Water Height: 21' 2"

<u>Lattice Position</u>	<u>Run #</u>	<u>Gauge Air Pressure (Cm. Hg.)</u>	<u>Control Rod (In.)</u>	<u><math>\Delta k/k(\%)</math></u>	<u>Flow Rate <math>\times 10^3</math> (ft<sup>3</sup>/sec)</u>	<u><math>\Delta v/v(\%)</math></u>
47	1	0.0	26 3/8	0.0	0.0	0.0
	2	55.9	25 3/8	0.020	0.630	0.0801
	3	60.0	24 31/32	0.028	1.05	0.1378
	4	64.2	24 15/32	0.039	1.40	0.1893
	5	70.4	23 7/8	0.050	1.82	0.2560
	6	75.5	23 11/16	0.054	2.05	0.2992
	7	83.9	23 3/16	0.064	2.29	0.3530
	8	91.4	23	0.066	2.44	0.3940
57	1	0.0	25 11/32	0.0	0.0	0.0
	2	55.9	24 15/32	0.018	0.630	0.0801
	3	60.0	24 5/32	0.023	1.05	0.1378
	4	64.2	23 25/32	0.031	1.40	0.1893
	5	70.4	23 11/32	0.039	1.82	0.2560
	6	75.5	23 5/32	0.043	2.05	0.2992
	7	83.9	22 27/32	0.049	2.29	0.3530
	8	91.4	22 11/16	0.053	2.44	0.3940
25	1	0.0	25 1/32	0.0	0.0	0.0
	2	55.9	23 31/32	0.022	0.630	0.0801
	3	60.0	23 9/16	0.030	1.05	0.1378
	4	64.2	23 1/4	0.036	1.40	0.1893
	5	70.4	22 23/32	0.047	1.82	0.2560
	6	75.5	22 7/16	0.052	2.05	0.2992
	7	83.9	22 3/32	0.059	2.29	0.3530
	8	91.4	21 13/16	0.064	2.44	0.3940

Exp. #64, Barometer: 75.1 cm. Hg., Water Height: 21' 1/2"

<u>Lattice Position</u>	<u>Run #</u>	<u>Gauge Air Pressure (Cm. Hg.)</u>	<u>Control Rod (In.)</u>	<u><math>\Delta k/k(\%)</math></u>	<u>Flow Rate <math>\times 10^3</math> (ft<sup>3</sup>/sec)</u>	<u><math>\Delta v/v(\%)</math></u>
48	1	0.0	20 7/8	0.0	0.0	0.0
	2	55.7	20 7/32	0.010	0.630	0.0800
	3	59.7	19 3/4	0.020	1.04	0.1363
	4	64.0	19 13/32	0.026	1.43	0.1937
	5	70.2	19 1/8	0.029	1.82	0.2565
	6	75.3	18 15/16	0.032	2.12	0.3150
	7	83.7	18 19/32	0.037	2.29	0.3525
	8	91.2	18 7/16	0.039	2.44	0.3950
	9	64.0	19 5/16	0.026	1.43	0.1937
	10	59.7	19 5/8	0.021	1.04	0.1363
55	1	0.0	20 9/32	0.0	0.0	0.0
	2	55.7	18 5/8	0.025	0.630	0.0800
	3	59.7	17 5/8	0.039	1.04	0.1363
	4	64.0	16 29/32	0.047	1.43	0.1937
	5	70.2	15 23/32	0.058	1.82	0.2565
	6	75.3	14 11/16	0.066	2.12	0.3150
	7	83.7	12 19/32	0.074	2.29	0.3525

Exp. #65, Barometer: 75.3 cm. Hg., Water Height: 21'

<u>Lattice Position</u>	<u>Run #</u>	<u>Gauge Air Pressure (Cm. Hg.)</u>	<u>Control Rod (In.)</u>	<u><math>\Delta k/k(\%)</math></u>	<u>Flow Rate <math>\times 10^3</math> (ft<sup>3</sup>/sec)</u>	<u><math>\Delta v/v(\%)</math></u>
53	1	0.0	22 15/16	0.0	0.0	0.0
	2	55.7	22 1/8	0.016	0.630	0.0802
	3	59.7	21 13/16	0.023	1.05	0.1378
	4	64.0	21 11/16	0.025	1.41	0.1908
	5	70.2	21 5/16	0.031	1.83	0.2580
	6	75.3	21	0.039	2.13	0.3150
	7	83.7	20 13/16	0.041	2.32	0.3600
	8	91.2	20 11/16	0.043	2.45	0.3960

Exp. #54, Barometer: 75.3 cm. Hg., Water Height: 21' 3"

35	1	0.0	25 21/32	0.0	0.0	0.0
	2	53.0	25 1/8	0.011	0.250	0.0282
	3	56.2	24 9/16	0.023	0.650	0.0750
	4	59.1	24 9/16	0.031	0.950	0.1180
	5	64.2	23 7/16	0.045	1.38	0.1690
	6	71.6	22 5/8	0.061	1.92	0.2479
	7	76.7	22 1/4	0.068	2.08	0.2778
	8	83.7	22 1/16	0.072	2.27	0.3170
	9	96.4	21 7/16	0.083	2.51	0.3780
	10	75.2	22 1/2	0.064	2.03	0.2680
	11	61.6	23 5/8	0.041	1.16	0.1396
	12	54.5	24 5/8	0.021	0.450	0.0513

NOTE: Exp. #54 was done with the Wet Test Meter in the line. Therefore 10% correction factor to void ratio calculation was not applied.







UNIVERSITY OF MICHIGAN



**3 9015 03525 0300**